DOI: 10.1002/jnr.24954

RESEARCH ARTICLE

Neuroscience Research

Osteopontin regulates proliferation, migration, and survival of astrocytes depending on their activation phenotype

Sabine Ulrike Vay¹ | Daniel Navin Olschewski¹ | Helena Petereit¹ | Felix Lange¹ | Nilufar Nazarzadeh¹ | Elena Gross¹ | Monika Rabenstein¹ | Stefan Johannes Blaschke^{1,2} | Gereon Rudolf Fink^{1,2} | Michael Schroeter^{1,2} | Maria Adele Rueger^{1,2}

Correspondence

Sabine Ulrike Vay, Department of Neurology, Faculty of Medicine and University Hospital Cologne, University of Cologne, Kerpener Str. 62, Cologne 50924, Germany. Email: sabine.vay@uk-koeln.de

Funding information

The "Köln Fortune Program"/Faculty of Medicine, University of Cologne, Germany (345/2018) and the "Marga-und-Walter-Boll-Foundation" (#210-10-15) supported this study. HP received additional funding by the "Köln Fortune Program"/Faculty of Medicine, University of Cologne, Germany (334/2019). GRF, MS, and MAR are funded by the Deutsche Forschungsgemeinschaft (DFG, German Research Foundation)—Project-ID 431549029 – SFB 1451

Abstract

The glycoprotein osteopontin is highly upregulated in central nervous system (CNS) disorders such as ischemic stroke. Osteopontin regulates cell growth, cell adhesion, homeostasis, migration, and survival of various cell types. Accordingly, osteopontin is considered an essential regulator of regeneration and repair in the ischemic milieu. Astrocytes are the most abundant cells in the CNS and play significant roles in health and disease. Astrocytes are involved in homeostasis, promote neuroprotection, and regulate synaptic plasticity. Upon activation, astrocytes may adopt different phenotypes, termed A1 and A2. The direct effects of osteopontin on astrocytes, especially in distinct activation states, are yet unknown. The current study aimed to elucidate the impact of osteopontin on resting and active astrocytes. We established an inflammatory in vitro model of activated (A1) primary astrocytes derived from neonatal wistar rats by exposure to a distinct combination of proinflammatory cytokines. To model ischemic stroke in vitro, astrocytes were subjected to oxygen and glucose deprivation (OGD) in the presence or absence of osteopontin. Osteopontin modulated the activation phenotype by attenuating A1- and restoring A2-marker expression without compromising the active astrocytes' immunocompetence. Osteopontin promoted the proliferation of active and the migration of resting astrocytes. Following transient OGD, osteopontin mitigated the delayed ongoing death of primary astrocytes, promoting their survival. Data suggest that osteopontin differentially regulates essential functions of resting and active astrocytes and confirm a significant regulatory role of osteopontin in an in vitro ischemia model. Furthermore, the data suggest that osteopontin constitutes a promising target for experimental therapies modulating neuroregeneration and repair.

KEYWORDS

A1, A2, activation, astrocytic C3 staining, CC3, cerebral ischemia, complement component 3, cytokine mix, neuroinflammation, OGD, OPN, RRID: AB_10544537, RRID: AB_10981081,

Edited by Christopher Anderson and Junie Warrington. Reviewed by Hiroko Ikeshima-Kataoka and Andre Obenaus.

This is an open access article under the terms of the Creative Commons Attribution-NonCommercial-NoDerivs License, which permits use and distribution in any medium, provided the original work is properly cited, the use is non-commercial and no modifications or adaptations are made.

© 2021 The Authors. *Journal of Neuroscience Research* published by Wiley Periodicals LLC.

2822

¹Department of Neurology, Faculty of Medicine and University Hospital Cologne, University of Cologne, Cologne, Germany

²Cognitive Neuroscience, Institute of Neuroscience and Medicine (INM-3), Research Centre Juelich, Juelich, Germany

RRID: AB_10983078, RRID: AB_11012229, RRID: AB_11181928, RRID: AB_11212597, RRID: AB_2224402, RRID: AB_330713, RRID: AB_331765, RRID: AB_476811, RRID: AB_476857, RRID: AB_94843, \$100A10, \$100A10 staining, \$PP1

1 | INTRODUCTION

Osteopontin, also named secreted phosphoprotein 1 (SPP1), is an endogenous phosphoglycoprotein ubiquitously expressed in the CNS. It is classified as a component of the extracellular matrix (ECM) and as a soluble cytokine. Osteopontin regulates cell growth, cell adhesion, homeostasis, migration, and survival of various cell types (Briones-Orta et al., 2017; Huang et al., 2017; Oyama et al., 2018; Rabenstein et al., 2015; Rogall et al., 2018). Moreover, osteopontin plays a role in various CNS diseases via modulating inflammatory responses (Giachelli & Steitz, 2000; Rabenstein et al., 2016), promoting repair (Ladwig et al., 2019; Rogall et al., 2018; Schroeter et al., 2006), supporting neuroprotection, and restoring the bloodbrain barrier (Gliem et al., 2015; Rabenstein et al., 2016; Suzuki et al., 2010). Osteopontin is upregulated with striking abundance in the acute phase after ischemic stroke, brain injury, infection, or neoplasia (Brown et al., 2011; Choi et al., 2007; Gliem et al., 2015; Jin et al., 2006; Rakers et al., 2019; Riew et al., 2019; Szulzewsky et al., 2018). After a stroke, osteopontin is expressed by immigrating monocytes/macrophages and resident microglia (Gliem et al., 2015; Riew et al., 2019; Wang et al., 1998). We previously demonstrated that osteopontin counteracts the LPS-induced proinflammatory response of microglia in vitro and after ischemic stroke (Rabenstein et al., 2016), drives microglial polarization toward an antiinflammatory phenotype (Ladwig et al., 2017), and consequently reduces secondary neurodegeneration in the thalamus (Ladwig et al., 2019; Schroeter et al., 2006). Furthermore, osteopontin mediates the proliferation and migration of neural stem cells toward the lesion site after stroke (Rabenstein et al., 2019; Rogall et al., 2018).

In the past decades, astrocytes have attracted growing attention due to discovering their crucial and diverse roles in the central nervous system (CNS), far exceeding the outdated idea of a mere mechanical stabilization of the brain. As the most abundant cells of the CNS, they provide diverse homeostatic maintenance functions, promote neurotrophic support, and regulate synaptic plasticity (Chung et al., 2013; Clarke & Barres, 2013; Liddelow & Barres B: SnapShot, 2015; Sofroniew & Vinters, 2010). Astrocytes promptly react to any brain injury by adapting their morphology and gene expression and forming the glial scar (Anderson et al., 2016; Rolls et al., 2009; Stoll et al., 1998). Moreover, active astrocytes regulate neuroinflammation and secrete inflammatory cytokines (Falsig et al., 2004, 2006). Intriguingly, astrocytes have beneficial and detrimental effects on CNS regeneration (Anderson et al., 2016; Bush et al., 1999; Faulkner et al., 2004; Liddelow et al., 2017; Schroeter et al., 2009; Sofroniew, 2015; Song et al., 2002; Stevens et al., 2007). Depending on their expression profile, active astrocytes are categorized as A1- or A2-activated astrocytes (Liddelow et al., 2017). Gliem et al. (2015) suggested that osteopontin supports

Significance

- the characteristics and functions of active astrocytes differ substantially from resting astrocytes in vitro,
- osteopontin has a significant regulating impact on the characteristics and functions of resting and active astrocytes.

active astrocytes' functions *in vivo*, thereby stabilizing the blood-brain barrier after ischemic stroke.

Accordingly, astrocytes and osteopontin play valuable roles after brain injury. However, their interplay in health and disease remains elusive. To shed light on this issue, we aimed to evaluate the effects of osteopontin on astrocytes' key functions, depending on their activation state. Therefore, we established an *in vitro* model of primary astrocytes induced to display distinct resting versus active phenotypes and examined proliferation, migration, marker expression, morphology, and immunocompetence in the presence and absence of osteopontin.

2 | MATERIAL AND METHODS

2.1 | Animals

Animal procedures for tissue harvesting obeyed the German Federal Laws for Animal Protection. The local animal care committee (AZ UniKöln_Anzeige §4.16.021) approved the study. Wistar rats for breeding were maintained in polysulfone cages with sawdust bedding on a 12 hr light/dark cycle. Food and water were provided ad libitum in pathogen-free conditions. Six different litters maintained by two breeding pairs were used for the experiments, and all pups of each litter (9–15) were pooled for cultures independent of their sex.

2.2 | Astrocytes isolation and culture

Pure neonatal astrocytes cultures were obtained from the cortices of neonatal Wistar rats (P1–P3). Rat cortices were incubated in trypsin/EDTA solution (1% trypsin, 0.02% EDTA) for 15 min at 37°C. The addition of the culture medium (Dulbeccos essential medium (DMEM) with the addition of 10% fetal calf serum (FCS), 1% penicillin/streptomycin, and 2 mM L-glutamine) stopped the reaction. The cortices were dissociated by repeated up- and down-pipetting. The resulting cell suspension was centrifuged at 1,200 rpm for 2 min. Cells were resuspended in DMEM (10% FCS, 1% penicillin/

streptomycin, and 2 mM L-glutamine) and grown at 37°C with 5% CO2 for 8 to 10 days. The culture medium was changed after the third day. This prolonged cultivation approach promoted a selective growth of astrocytes and microglia. Culture flasks were shaken at least three times for 1 hr at 250 rpm on an orbital shaker (37°C), detaching microglia from the adherent astrocyte layer. This procedure removed microglia from the initial co-culture. The medium containing detached microglia was disposed of. The remaining astrocytes were detached using trypsin/EDTA solution (0.05% trypsin, 0.02% EDTA) for 15 min at 37°C and centrifuged for 2 min at 1,200 rpm, yielding a pure astrocyte pellet that was resuspended in fresh culture medium and sown into subcultures. All experiments were performed with these purified astrocytes cultures. One to 3 days after seeding astrocytes in a subculture (at a density of 260 cells/mm² or for ATP assay, migration scratch and live/dead assay 624 cells/ mm²), cells were used for further experiments. Astrocytes were left unstimulated (resting astrocytes, control), or were stimulated with cytokine mix (CM) containing recombinant rat TNF α (10 ng/ml), recombinant rat IL1β (5 ng/ml) and recombinant rat IFNγ (10 ng/ml; all from Peprotech, Hamburg, Germany), to obtain active astrocytes. We chose the combination of these cytokines because they are known to be upregulated under neuroinflammatory conditions, for example, after cerebral ischemia (Walberer et al., 2010). The doses of cytokines were chosen based on studies on immortalized and primary mouse astrocytes in vitro by Neal et al. (2018) and Matsumoto et al. (2012). Cells were treated with 5 or 10 µg/ml recombinant rat osteopontin (R&D systems, Minnesota Canada) to investigate the effects of osteopontin on astrocytes. The doses of osteopontin were chosen based on our previous studies investigating the effects of osteopontin on microglia and neural stem cells in vitro (Rabenstein et al., 2015, 2016). For some experiments, astrocytes were exposed to both CM plus osteopontin. All experiments were conducted in at least three biological triplicates that—in turn—were conducted with cell cultures out of at least three different litters.

2.3 | Griess assay

NO release from astrocytes was quantified by photometrical detection of NO using a Griess reagent kit (Biotium, Hayward, USA). Twenty-four hours after the last stimulation of astrocytes, the supernatant was collected, and the content of NO was measured following the manufacturer's protocol. The optical density (OD) of each sample was measured at 548 nm in a plate reader (FLUOstar Omega, BMG LABTECH, Ortenberg, Germany). Mean values \pm standard error of the mean (SEM) were established among equally treated samples. Each experiment was conducted in at least quadruplets.

2.4 | Enzyme-linked immunosorbent assays

Concentrations of the proinflammatory cytokines TNF α , IL1 β , and IL6 were measured in the supernatant of astrocytes 24 hr after the

last stimulation, using the rat TNF α , IL1ß, or IL6 DuoSet enzymelinked immunosorbent assay (ELISA) Kit (Cat# DY510-05, #DY501, #DY506; R&D systems, Minnesota Canada). IL10 and insulin-like growth factor 1 (IGF1), as antiinflammatory cytokines, were measured using the rat IL10 ELISA and the mouse/rat IGF1 Quantikine ELISA Kit (Ca# BMS629, Thermo Fisher Scientific, Waltham, USA and Cat# MG100, R&D systems, Minnesota Canada). Experiments were conducted according to the manufacturer's protocol. The OD of each sample was measured using a plate reader. Cytokine and IGF1 concentrations of the samples were calculated based on standard curves. Mean values \pm SEM were established among equally treated samples. Each experiment was conducted in at least triplicate.

2.5 | Real-time quantitative PCR

RNA from cultivated cells was isolated 24 or 72 hr after treatment using the GeneUP total RNA mini Kit (Biotechrabbit, Henningsdorf, Germany), following the manufacturer's protocol. Total RNA concentration and purity were evaluated photometrically. Total RNA (10 ng) was converted to cDNA by reverse transcription with the QuantiTect reverse transcription kit (Qiagen, Hilden, Germany), following the manufacturer's recommendations. All primers used in this study were obtained from Biolegio (Nijmegen, The Netherlands). Primer sequences and PCR parameters are listed in Table 1. The samples were amplified and quantified on a Bio-Rad CFX ConnectTM real-time system (Hercules, CA, USA) or LightCycler 96 (Roche, Mannheim, Germany). PCR product integrity was evaluated by melting point analysis and agarose gel electrophoresis. The threshold cycle (CT) was normalized to ribosomal protein L13a (RPL13a; ΔCT). Data are depicted as 2(- $\Delta\Delta$ CT). Real-time quantitative PCR (RT-qPCR) was performed in technical triplets, and each experiment was conducted in at least biological triplicate. Mean values \pm SEM were calculated for all samples.

2.6 | Live/dead assay

Cells were sown on 96-well plates and exposed to either CM or oxygen-glucose deprivation (OGD) versus control, in the presence or absence of osteopontin. Dead cells were stained with propidium iodide (Life Technologies, Darmstadt, Germany), and all cells, irrespective of viability, were counterstained with Hoechst 33342 (Life Technologies, Darmstadt, Germany). Representative pictures were taken using an inverted fluorescence phase-contrast microscope. Ten images per well were taken, and Hoechst-stained and propidium iodide-stained cells were counted manually. The ratio of propidium iodide positives on total cell count provided the proportion of cell death. The experiment was performed in at least triplicate with four wells per condition. The resulting mean values \pm SEM were established among equally treated samples.

TABLE 1 Primers and parameters of RT-qPCR

| | Sequences forward/reversed | Temperature (°C) | Duration (s) | |
|---------------------|--|------------------|--------------|------------------|
| RNA | 5′-3′ | Step 1/2/3 | Step 1/2/3 | Accession number |
| GFAP | TGCATGTACGGAGTATCGCC/ GGGGGAGGAAAGGACAACTG | 95/60/72 | 15/15/45 | NM_017009.2 |
| vimentin | GCAGCCTCTATTCCTCGTCC/ TAGTTGGCGAAGCGGTCATT | 95/60/72 | 15/15/45 | NM_031140.1 |
| osteopontin | CCAGCCAAGGACCAACTACA/ AGTGTTTGCTGTAATGCGCC | 95/60/72 | 15/15/45 | NM_012881.2 |
| S100A10 | CACACCTTGATGCGTCCTCT/ GGCAACCGGATGCAAACAAT | 95/60/72 | 15/15/45 | NM_031114.1 |
| complement C3 (CC3) | ATCGAGGATGGTTCAGGGGA/ GCCTCTACCATGTCGCTACC | 95/60/72 | 15/15/45 | NM_016994.2 |
| ΤΝΓα | CATCCGTTCTCTACCCAGCC/ AATTCTGAGCCCGGAGTTGG | 95/56.6/72 | 15/15/45 | NM_012675.3 |
| IL-6 | CCCAACTTCCAATGCTCTCCT/ AGCACACTAGGTTTGCCGAG | 95/57.3/72 | 15/15/45 | NM_012589.2 |
| ΙL1-β | GACTTCACCATGGAACCCGT/ GGAGACTGCCCATTCTCGAC | 95/56/72 | 15/15/45 | NM_031512.2 |
| IL-10 | GAAAAATTGAACCACCCGGCA/ TTTCCAAGGAGTTGCTCCCG | 95/56/72 | 15/15/45 | NM_012854.2 |
| connexin 43 | CTCACGTCCCACGGAGAAAA/ CGCGATCCTTAACGCCTTTG | 95/60/72 | 15/15/45 | NM_012567.2 |
| iNOS | GCTTGTCTCTGGGTCCTCTG/ CTCACTGGGACAGCACAGAA | 95/59.0/72 | 15/15/45 | NM_012611.3 |
| Ki67 | TCTTGGCACTCACAGTCCAG/ GCTGGAAGCAAGTGAAGTCC | 95/58.0/72 | 15/15/45 | NM_001271366.1 |
| RPL13a | TCTCCGAAAGCGGATGAACA/ CAACACCTTGAGGCGTTCCA | | 15/15/45 | NM_173340.2 |

2.7 | Bromodeoxyuridine proliferation assay

Bromodeoxyuridine (BrdU; Cayman Chemical Company, Michigan, USA) served to label and quantify proliferating astrocytes. Cells were sown on 24-well plates with glass coverslips inside the wells. Eighteen hours after treatment with CM and osteopontin, 10 μ M BrdU were added to each well. After 6 hr of incubation, the experiment was stopped by cell fixation with 4% PFA, and cells were stained for incorporated BrdU (see below). Ten pictures of each sample were taken using an inverted fluorescence phase-contrast microscope, and at least 250 total cells per sample and experiment were counted manually. The ratio of BrdU-positive cells on total cell count provided the proportion of proliferating cells. The experiment was performed in triplicate with two wells per condition. The resulting mean values \pm SEM were established among equally treated samples.

2.8 | Immunocytochemistry

All antibodies used in this study are listed in Table 2. Staining against Glial Fibrillary Acidic Protein Antibody (GFAP; clone GA5, mouse monoclonal antibody, dilution 1:500, Cat# MAB360, Merck, Darmstadt, Germany; RRID: AB_11212597) was used to identify

astrocytes. Marking the cytoskeleton of cells by anti-vimentin (clone V9, mouse monoclonal antibody, dilution 1:250, Cat#MAB3400, Merck Darmstadt, Germany; RRID:AB_94843) identified the shape of cells. The purity of astrocytes cultures was regularly verified by conducting co-stainings with anti-GFAP and anti-ionized calciumbinding adapter molecule 1 (lba1; goat polyclonal antibody, dilution 1:500, Cat# ab5076, Abcam, Milton, UK; RRID: AB_2224402) to detect microglia and allowing a maximal fraction of microglia <10%. Anti-complement component 3 (CC3, clone 12E2, mouse monoclonal antibody, dilution 1:500, Cat# HYB118-02, Thermo Fisher Scientific, Waltham, USA; RRID: AB 11181928) was used to identify the activated A1 phenotype of astrocytes. Anti-S100A10 (polyclonal rabbit antibody, dilution 1:50, Cat#NBP1-89370, Novus, Centennial, USA; RRID: AB_11012229) detected the A2 astrocytic phenotype. The translocation of resting NFκB from the cytoplasm into the cell nuclei of active astrocytes was identified using anti-NFκB p65 (rabbit polyclonal antibody, dilution for ICC and western blot 1:500, Cat#PA5-16545, Thermo Fisher Scientific, Waltham, USA; RRID: AB_10981081). Hemichannels of astrocytes, mainly composed of connexin-43 (CX43) protein, were detected by anti-CX43, (rabbit polyclonal antibody, dilution 1:8,000, Cat#C6219, Sigma Aldrich, St. Louis, USA; RRID: AB_476857). Astrocytes were stained with anti-BrdU (clone BU-33, mouse monoclonal, dilution 1:200, Cat# B8434,

TABLE 2 Primary and secondary antibodies

| Mouse anti- BRDU clone BU-33 clone 12E2 Bromodeoxyuridine conjugated to KLH BRD-84 A/8811 Sigma Aldrich, Cath BRD-84 A/8811 Primary, monoclonal Primary, monoclonal Cath FIVBIR-8-02 RRID: AB, 478817 1:200 Primary, monoclonal Cath FIVBIR-8-02 RRID: AB, 1181928 Primary, monoclonal Primary, monoclonal Cath FIVBIR-8-02 RRID: AB, 1181928 Primary, monoclonal Primary, monoclonal Cath FIVBIR-8-02 RRID: AB, 278887 1:8,000 RRID: AB, 478887 Mouse anti- GFAP, clone GAS Purified GFAP from porcine spinal cord GFAP, clone GAS Morck Millipore, Cath AB, 800 RRID: AB, 11212597 Primary, monoclonal Bridge Five Five Five Five Five Five Five Fiv | | , | | | |
|--|----------------------------------|---|--------------------|-----------------------|----------|
| BB1032 Spring Sp | Antibody name | Immunogen structure | Origin | Туре | Dilution |
| Mouse anti-CC3, clone 12E2 Rabbit anti-CX43 Synthetic peptide corresponding to the C-terminal segment of the cytoplasmic domain famino acids with N-terminally added byting) of humanyrat connexin-43 Mouse anti-CG4, clone CA5 Rabbit anti-CX43 Synthetic peptide corresponding to the C-terminal segment of the cytoplasmic domain famino acids with N-terminally added byting) of humanyrat connexin-43 Mouse anti-CG4R, clone CA5 Rabbit anti-Histone H3 XP® (DH12) Synthetic peptide corresponding to the C-terminal of the human histone H3 protein which was a connexin-43 Rabbit anti-Histone H3 XP® (DH12) Synthetic peptide corresponding to human libral as 135-147 (C terminal): Sequence: C167PPAKKA1SELP Synthetic peptide from the C-terminal of C167PPAKKA1SELP Rabbit anti-posopho-PaR MAPK Synthetic peptide corresponding to residues surrounding psers36 of human NFkB p65 Rabbit anti-psa MAPK Synthetic peptide corresponding to residues surrounding psers36 of human NFkB p65 Rabbit anti-psa MAPK Synthetic peptide corresponding to residues surrounding Psers36 of human NFkB p65 Rabbit anti-psa MAPK Rabbit anti | BRDU, clone | Bromodeoxyuridine conjugated to KLH | • | Primary, monoclonal | 1:200 |
| Rabbit anti-CX43 Synthetic peptide corresponding to the C-terminal segment of the cytoplasmic domain (anino acids with N-terminally added lysine) of human/rat connexin-43 Merck Millipore, Catil Ag. 476857 RRID: AB. 476857 RRID: | BU-33 | | RRID: AB_476811 | | |
| Rabbit anti- CX43 Synthetic peptide corresponding to the C-terminal segment of the cytoplasmic domain domino acids with N-terminally added lysine) of human/rat connexin-43 Mouse anti- GFAP, clone GAS Rabbit anti- Histone H3 XP® (D1H2) Goat anti- Iba1 Synthetic peptide corresponding to the C-terminal of the human histone H3 protein bland as 135-147 (C terminal). Sequence: C-TGPPAKRAISELP Rabbit anti- Histone H3 XP® (D1H2) Goat anti- Iba1 Synthetic peptide corresponding to human load as 135-147 (C terminal). Sequence: C-TGPPAKRAISELP Rabbit anti- Histone H3 XP® (D1H2) Goat anti- Iba1 Synthetic peptide corresponding to human load as 135-147 (C terminal). Sequence: C-TGPPAKRAISELP Rabbit anti- Histone H3 XP® (D1H2) Synthetic peptide corresponding to residues surrounding pSer536 of human NFk8 p65 Rabbit anti- p38 MAPK Rabbit anti- p | | C3 purified from rat serum | | Primary, monoclonal | 1:500 |
| segment of the cytoplasmic domain damino acids with N-terminally added lysine) of human/rat connexin-43 Mouse anti-GFAP, clone GA5 Rabbit anti-Histone H3 XP8 (D1H2) Goat anti-Iba1 Synthetic peptide corresponding to the C-terminal of the human histone H3 protein histone H3 protein Synthetic peptide corresponding to human histone H3 protein AB 1,0544537 Synthetic peptide corresponding to human histone H3 protein Synthetic peptide corresponding to human histone H3 protein AB 1,0544537 Goat anti-Iba1 Synthetic peptide corresponding to human histone H3 protein C-TGPPAKRAISELP Rabbit anti-NFGB Synthetic peptide corresponding to human NFKappaB protein NFKappaB Synthetic peptide corresponding to residues surrounding pSer536 of human NFKappaB (RID: AB 1,0981081) Rabbit anti-phospho-NFKB p65 RABbit anti-p38 MAPK Synthetic peptide corresponding to the sequence of human p38 MAPK Synthetic peptide corresponding to residues surrounding pSer536 of human p38 MAPK Cat#6212 Rabbit anti-phospho-pa38 MAPK Synthetic peptide corresponding to residues surrounding Thr180/Tyr182 of human p38 MAPK RID: AB 1,0983078 Rabbit anti-phospho-pa38 MAPK Synthetic phospho-peptide corresponding to residues surrounding Thr180/Tyr182 of human p38 MAPK RID: AB 3,30713 Rabbit AB Recombinant protein corresponding to amino acids: MAPK Synthetic phospho-pa38 MAPK RID: AB 3,31765 Rabbit AB Recombinant protein corresponding to amino acids: MAPK RID: AB 3,31765 Rabbit AB Recombinant protein corresponding to amino acids: MAPK RID: AB 3,31765 Rabbit AB Recombinant protein corresponding to amino acids: MAB RID: AB 2,34104 Rabbit AB Recombinant protein corresponding to amino acids: MAB RID: AB 2,34104 Rabbit AB Recombinant protein corresponding to amino acids: MAB RID: AB 2,34104 Rabbit AB Recombinant protein corresponding to amino acids: MAB RID: AB 2,441057 RRID: AB 2,441057 RRID: AB 2,441057 RRID: AB 2,534104 RRID: AB 2, | | | RRID: AB_11181928 | | |
| GA5 RID: AB_11212597 Rabbit anti-Histone H3 Protein C- terminal of the human histone H3 protein C- terminal of the human h35-147 (C terminal); Sequence: C-T-GPAKA15E10 RRID: AB_22224402 C- terminal the human h35-147 (C terminal); Sequence: C-T-GPAKA15E16545, RRID: AB_2224402 C- terminal the human p35 terminal possible passible passible protein corresponding to residues phospho-phosphospho-phospho-phosphospho-phosphosphospho-phospho-phosphosphosphosphosphosphosphosphosp | Rabbit anti-CX43 | segment of the cytoplasmic domain (amino acids with N-terminally added lysine) of human/rat | | Primary, polyclonal | 1:8,000 |
| Rabbit anti- Histone H3 XP® (D1H2) Goat anti-Iba1 Synthetic peptide corresponding to the C- terminal of the human histone H3 protein XP® (D1H2) Goat anti-Iba1 Synthetic peptide corresponding to human Iba1 as 135-147 (C terminal); Sequence: CTGPPARK AISELP Rabbit anti-NFxB p65 Rabbit anti-NFxB p65 Rabbit anti-p38 protein Rabbit anti-p38 MAPK Rabbit anti-p198 Synthetic peptide corresponding to the sequence of human p38 MAPK Rabbit anti-p38 Synthetic protection corresponding to the sequence of human p38 MAPK Rabbit anti-p38 MAPK Rabbit anti-p38 MAPK Rabbit anti-p38 MAPK Rabbit anti-p38 Synthetic phosphopeptide corresponding to residues surrounding Thr180/Tyr182 of human p38 MAPK Rabbit anti-p38 MAPK Rabbit anti-p38 MAPK Rabbit anti-p38 MAPK Rabbit anti-p38 Synthetic phosphopeptide corresponding to residues surrounding Thr180/Tyr182 of human p38 MAPK Rabbit anti-p38 MAPK Rabbit anti-p38 MAPK Rabbit anti-p38 Synthetic phosphopeptide corresponding to residues surrounding Thr180/Tyr182 of human p38 MAPK Rabbit anti-p38 MAPK Rabbit anti-p38 MAPK Rabbit anti-p38 Synthetic phosphopeptide corresponding to residues surrounding Thr180/Tyr182 of human p38 MAPK Rabbit anti-p38 MAPK Rabbit anti-p38 MAPK Rabbit anti-p38 Synthetic phosphopeptide corresponding to residues surrounding Thr180/Tyr182 of human p38 MAPK Rabbit anti-p38 MAPK | GFAP, clone | Purified GFAP from porcine spinal cord | MAB360 | Primary, monoclonal | 1:500 |
| Histone H3 XPs (D1H2) the human histone H3 protein AB_10544537 Goat anti-Iba1 Synthetic peptide corresponding to human Iba1 as 135-147 (C terminal); Sequence: C-TCPPAKK AISELP RRID: AB_2224402 RRID: AB_10981081 Rabbit anti-PASS Synthetic peptide from the C-terminus of human NFkappaB protein NFkappaB protein Surrounding pSer536 of human NFkB p65 RRID: AB_10981081 Rabbit anti-PASS Synthetic peptide corresponding to residues surrounding pSer536 of human NFkB p65 RRID: AB_10983078 Rabbit anti-PASS MAPK RRID: AB_10983078 RRID: AB_10983078 RRID: AB_330713 Cell Signaling Technology, Catt#4631 RRID: AB_330713 Cell Signaling Technology, Catt#46431 RRID: AB_333763 RRID: AB_330713 RRID: AB_331765 RRID: AB_331765 RRID: AB_10112229 RRID: AB_101122 | | | _ | D: 1 | 4.4.000 |
| Ibat aa 135-147 (C terminal); Sequence: | Histone H3 | | Cat#4499, RRID: | Primary, monocional | 1:1,000 |
| Rabbit anti-NFKB p65 Rabbit anti-phospho-NFKB p65 Rabbit anti-pass market peritide corresponding to residues surrounding p5er536 of human NFKB p65 Rabbit anti-pass MAPK Rabbit anti-pass more phospho-pass wire phos | Goat anti- Iba1 | Synthetic peptide corresponding to human | Abcam, Cat# ab5076 | Primary, polyconal | 1:500 |
| Primary, monoclonal surrounding pSer536 of human NFkB p65 RRID: AB_10981081 Rabbit anti-phospho-NFkB p65 Rabbit anti-p38 MAPK Rabbit anti-p38 MAPK Rabbit anti-p4 Synthetic peptide corresponding to residues numan p38 MAPK Rabbit anti-p38 MAPK Rabbit anti-p38 MAPK Rabbit anti-p4 Synthetic peptide corresponding to the sequence of human p38 MAPK Rabbit anti-p4 Synthetic phosphopeptide corresponding to residues surrounding Thr180/Tyr182 of human p38 MAPK Rabbit anti-p4 Synthetic phosphopeptide corresponding to residues surrounding Thr180/Tyr182 of human p38 MAPK Rabbit anti-p5100A10 Recombinant protein corresponding to amino acids: MPSQMEHAMETMMFTFHKFAGDKGYLTKED LRVLMEKEFPGFLENQKDPLAVDKIMKDLDQCRDGKV Mouse anti-vimentin, clone V9 Robert anti-Mouse Aritify (H+L), Alexa Fluor 568 Goat anti-Mouse Again immunoglobins heavy and light chains [IgG (H+L), Alexa Fluor 488 Goat anti-Mouse Gamma immunoglobins heavy and light chains [IgG (H+L), Alexa Fluor 488 Goat anti-Rabbit IgG (H+L), Alexa Fluor 568 Goat anti-Rabbit IgG (AH+L), Alexa Fluor 568 Robert Alto Gamma immunoglobins heavy and light chains Ribbit IgG (AH+L), Alexa Fluor 568 Robert Alto Gamma immunoglobins heavy and light chains Ribbit IgG (AH+L), Alexa Fluor 568 Robert Alto Gamma immunoglobins heavy and light chains Ribbit IgG (AH+L), Alexa Fluor 568 Robert Alto Gamma immunoglobins heavy and light chains Ribbit IgG (AH+L), Alexa Fluor 568 Robert Alto Gamma immunoglobins heavy and light chains Ribbit IgG (AH+L), Alexa Fluor 568 Robert Alto Gamma immunoglobins heavy and light chains Ribbit IgG (AH+L), Alexa Fluor 568 Robert Alto Gamma immunoglobins heavy and light chains Ribbit IgG (RH+L), Alexa Fluor 568 Robert Alto Ribbit IgG (RH+L), Alexa Fluor 56 | | · · · · · · · · · · · · · · · · · · · | RRID: AB_2224402 | | |
| Rabbit anti- phospho- NFxB p65 Rabbit anti- phospho- NFxB p65 Rabbit anti-p38 MAPK Synthetic peptide corresponding to residues aurrounding pSer536 of human NFkB p65 RRID: AB_10983078 Rabbit anti-p38 MAPK Synthetic peptide corresponding to the sequence of human p38 MAPK RRID: AB_300713 Rabbit anti- phospho-p38 MAPK Rabbit anti- S100A10 Recombinant protein corresponding to amino acids: MPSQMEHAMETIMMFTFHKFAGDKGYLTKED LRVLMEKEFPGFLENQKDPLAVDKIMKDLDQCRDGKV Mouse anti- simentin, clone V9 RRID: AB_331765 Novus, Cat#NBP1-89370, RRID: AB_11012229 Primary, monoclonal 1:500 RRID: AB_11012229 Primary, polyclonal 1:500 RRID: AB_11012229 Primary, monoclonal 1:200 RRID: AB_21011229 Primary, monoclonal 1:200 RRID: AB_2101229 Primary, monoclonal 1:200 RRID: AB_2101229 Primary, monoclonal 1:200 RRID: AB_2101229 Primary, monoclonal 1:200 RR | | | | Primary, polyclonal | 1:500 |
| phospho-NFkB p65 Rabbit anti-p38 MAPK Synthetic peptide corresponding to the sequence of human p38 MAPK Rabbit anti-p38 MAPK Rabbit anti-p38 MAPK Rabbit anti-p4 phospho-p38 MAPK Rabbit anti-p598 MAPK Rabbit anti-p698 MAPK Rabbit anti-s100A10 Recombinant protein corresponding to amino acids: MPSQMEHAMETMMETEHKEAGDKGYLTKED LRVLMEKEFPGFLENQKDPLAVDKIMKDLDQCRDGKV Mouse anti-s100A10 Recombinant protein corresponding to amino acids: MPSQMEHAMETMMETEHKEAGDKGYLTKED LRVLMEKEFPGFLENQKDPLAVDKIMKDLDQCRDGKV Mouse anti-s100A10 Recombinant protein corresponding to amino acids: MPSQMEHAMETMMETEHKEAGDKGYLTKED LRVLMEKEFPGFLENQKDPLAVDKIMKDLDQCRDGKV Mouse anti-s100A10 RRID: AB_94843 Primary, monoclonal 1:50 RRID: AB_94843 Primary, monoclonal 1:250 RRID: AB_94843 Primary, monoclonal 1:200 RRID: AB_9534104 Primary, monoclonal 1:200 RRID: AB_9534104 Primary, monoclonal 1:200 RRID: AB_9534104 Primary, monoclonal 1:200 RRID: AB_2534104 Primary, monoclonal 1:200 RRID: AB_9534104 Primary, monoclonal 1:200 RRID: AB_10112229 Primary, monoclonal 1:200 RRID: AB_10112229 Primary, mon | | | RRID: AB_10981081 | | |
| Rabbit anti-p38 MAPK MAPK Synthetic peptide corresponding to the sequence of human p38 MAPK Rabbit anti-p48 MAPK Rabbit anti-p58 MAPK Rabbit anti-p698 MAPK Rabbit anti-p698 MAPK Rabbit anti-s100A10 Recombinant protein corresponding to amino acids: | phospho- | | | Primary, monoclonal | 1:1,000 |
| MAPK Muman p38 MAPK Rabbit antiphospho-p38 MAPK Rabbit anti-S100A10 Recombinant protein corresponding to amino acids: MPSQMEHAMETMMFTFHKFAGDKGYLTKED LRVLMEKEFPGFLENQKDPLAVDKIMKDLDQCRDGKV MOuse antiphospho-p38 MAPK Rabbit anti-S100A10 Recombinant protein corresponding to amino acids: MPSQMEHAMETMMFTFHKFAGDKGYLTKED LRVLMEKEFPGFLENQKDPLAVDKIMKDLDQCRDGKV MOUSE antiphospho-p38 Maps antiphosphosphosphosphosphosphosphosphosphos | | | RRID: AB_10983078 | | |
| Rabbit anti- phospho-p38 MAPK Rabbit anti- phospho-p38 MAPK Rabbit anti- S100A10 Recombinant protein corresponding to amino acids: AMPSQMEHAMETMMFTFHKFAGDKGYLTKED LRVLMEKEFPGFLENQKDPLAVDKIMKDLDQCRDGKV Mouse anti- vimentin, clone V9 Purified vimentin from pig eye lens Ward (H + L), Alexa Fluor 568 Goat anti-Mouse lgG (H + L) Alexa Fluor 568 Goat anti-Rabbit lgG (H + L), Alexa Fluor 568 Goamma immunoglobins heavy and light chains Goat anti-Rabbit lgG (H + L), Alexa Fluor 568 Goamma immunoglobins heavy and light chains Goat anti-Rabbit lgG (H + L), Alexa Fluor 568 Goamma immunoglobins heavy and light chains Goat anti-Rabbit lgG (H + L), Alexa Fluor 568 Goamma immunoglobins heavy and light chains Goat anti-Rabbit lgG (H + L), Alexa Fluor 568 Goamma immunoglobins heavy and light chains Goamma immunoglobins heavy and light chains Thermo Fisher Scientific, Cat# A11001 RRID: AB_2534069 RRID: AB_2534069 Secondary, polyclonal 1:200 Cat# A21206, RRID: AB_2535792 | | | | Primary, polyclonal | 1:500 |
| Phospho-p38 MAPK MAPK RRID: AB_331765 Rabbit anti- S100A10 RPSQMEHAMETMMFTFHKFAGDKGYLTKED LRVLMEKEFPGFLENQKDPLAVDKIMKDLDQCRDGKV Mouse anti- vimentin, clone V9 Donkey anti- Goat IgG (H + L), Alexa Fluor 488 Goat anti-Rabbit IgG (H + L), Alexa Fluor 568 Consider a fluor 568 Gamma immunoglobins heavy and light chains Gamma immunoglobins heavy and light chains Thermo Fisher Scientific, Cat# A11001 RRID: AB_2534104 Cat# A11001 RRID: AB_2534069 RRID: AB_2534069 RRID: AB_143157 RRID: AB_143157 RRID: AB_143157 RRID: AB_2535792 Primary, polyclonal 1:200 RRID: AB#9370, RRID: | | | RRID: AB_330713 | | |
| Rabbit anti- S100A10 Recombinant protein corresponding to amino acids: AMPSQMEHAMETMMFTFHKFAGDKGYLTKED LRVLMEKEFPGFLENQKDPLAVDKIMKDLDQCRDGKV Mouse anti- vimentin, clone V9 Purified vimentin from pig eye lens MAB360 RRID: AB_94843 Donkey anti- Goat IgG (H + L), Alexa Fluor 568 Gamma immunoglobins heavy and light chains Fluor 488 Goat anti-Rabbit IgG (H + L), Alexa Fluor 568 Donkey anti- RRID: AB_2534069 RRID: AB_2534069 RRID: AB_2534069 Primary, monoclonal 1:250 RRID: AB_94843 Primary, monoclonal 1:200 Secondary, polyclonal 1:200 Cat# A11057 RRID: AB_2534104 Thermo Fisher Scientific, Cat# A11001 RRID: AB_2534069 Secondary, polyclonal 1:200 RRID: AB_2534069 Secondary, polyclonal 1:200 Cat#11011, RRID: AB_143157 RRID: AB_143157 Secondary, polyclonal 1:200 Cat# A21206, RRID: AB_2535792 | phospho-p38 | | | Primary, monoclonal | 1:500 |
| anti- \$100A10 MPSQMEHAMETMMFTFHKRAGDKGYLTKED LRVLMEKEFPGFLENQKDPLAVDKIMKDLDQCRDGKV Mouse antivimentin, clone V9 Purified vimentin from pig eye lens MAB360 RRID: AB_94843 Donkey anti- Goat IgG (H + L), Alexa Fluor 488 Goat anti-Rabbit IgG (H + L), Alexa Fluor 568 Donkey anti- Rabbit IgG (H + L), Alexa Fluor 568 Goamma immunoglobins heavy and light chains Thermo Fisher Scientific, Cat#A11001 RRID: AB_2534069 Donkey anti- Rabbit IgG (H + L), Alexa Fluor 568 Goamma immunoglobins heavy and light chains Thermo Fisher Scientific, Cat#11011, RRID: AB_143157 Donkey anti- Rabbit IgG (H + L), Alexa Fluor 568 Gamma immunoglobins heavy and light chains Thermo Fisher Scientific, Cat#A157 Thermo Fisher Scientific, Cat#11011, RRID: AB_143157 Secondary, polyclonal 1:200 | МАРК | | RRID: AB_331765 | | |
| vimentin, clone V9 RRID: AB_94843 Donkey anti-Goat IgG (H + L), Alexa Fluor 568 Goat anti-Rabbit IgG (H + L), Alexa Fluor 568 Donkey anti-Rabbit IgG (H + L), Alexa Fluor 568 Catma immunoglobins heavy and light chains Thermo Fisher Scientific, Cat# A11001 RRID: AB_2534069 RRID: AB_2534069 Catma immunoglobins heavy and light chains Thermo Fisher Scientific, Cat# A11001 RRID: AB_2534069 Catma immunoglobins heavy and light chains Thermo Fisher Scientific, Cat#11011, RRID: AB_143157 Cat# A121001 RRID: AB_143157 Cat# A21206, RRID: AB_2535792 | | MPSQMEHAMETMMFTFHKFAGDKGYLTKED | | Primary, polyclonal | 1:50 |
| Donkey anti- Goat IgG (H + L), Alexa Fluor 568 Goat anti-Mouse IgG (H + L) Alexa Fluor 488 Goat anti-Rabbit IgG (H + L), Alexa Fluor 568 Goat anti-Rabbit IgG (H + L), Alexa Fluor 568 Goat anti-Rabbit IgG (H + L), Alexa Fluor 568 Goat anti-Rabbit IgG (H + L), Alexa Fluor 568 Goat anti-Rabbit IgG (H + L), Alexa Fluor 568 Goamma immunoglobins heavy and light chains Thermo Fisher Scientific, Cat# A11001 RRID: AB_2534069 1:200 Cat#11011, RRID: AB_143157 Donkey anti- Rabbit IgG (H + L), Alexa RRID: AB_2535792 | | Purified vimentin from pig eye lens | • | Primary, monoclonal | 1:250 |
| Goat IgG (H + L), Alexa Fluor 568 Goat anti-Mouse IgG (H + L) Alexa Fluor 488 Goat anti-Rabbit IgG (H + L), Alexa Fluor 568 Goat mani-Mouse IgG (H + L) Alexa Fluor 488 Goat anti-Rabbit IgG (H + L), Alexa Fluor 568 Gamma immunoglobins heavy and light chains Cat# A11001 RRID: AB_2534069 Thermo Fisher Scientific, Cat#11011, RRID: AB_143157 Cat# A21206, RRID: AB_2535792 | clone V9 | | RRID: AB_94843 | | |
| Fluor 568 Goat anti-Mouse IgG (H + L) Alexa Fluor 488 Goat anti-Rabbit IgG (H + L), Alexa Fluor 568 Donkey anti-Rabbit IgG (H + L), Alexa Fluor 648 Goat anti-Rabbit IgG (H + L), Alexa Fluor 658 RRID: AB_2534069 Thermo Fisher Scientific, Cat#11011, RRID: AB_143157 Thermo Fisher Scientific, Secondary, polyclonal 1:200 Cat# A21206, RRID: AB_2535792 | Goat IgG (H + L), Alexa | Gamma immunoglobins heavy and light chains | • | Secondary, polyclonal | 1:200 |
| Goat anti-Mouse IgG (H + L) Alexa Fluor 488 Goat anti-Rabbit IgG (H + L), Alexa Fluor 568 Goat anti-Rabbit IgG (H + L), Alexa Fluor 68 Goat anti-Rabbit IgG (H + L), Alexa Fluor 68 Goat anti-Rabbit IgG (H + L), Alexa Fluor 68 Goat anti-Rabbit IgG (H + L), Alexa Fluor 68 Goat anti-Rabbit IgG (H + L), Alexa Fluor 68 Goat anti-Rabbit IgG (H + L), Alexa Fluor 68 Goat anti-Rabbit IgG (H + L), Alexa Fluor 68 Goat anti-Rabbit IgG (H + L), Alexa Fluor 68 Goat anti-Rabbit IgG (H + L), Alexa Fluor 68 Goat anti-Rabbit IgG (H + L), Alexa Fluor 69 Goat anti-Rabbit IgG (H + L), Alexa Fluor 60 RRID: AB_2535792 | | | RRID: AB_2534104 | | |
| 488 Goat anti-Rabbit IgG (H + L), Alexa Fluor 568 Donkey anti-Rabbit IgG (H + L), Alexa Fluor Rabbit IgG (H + L), Alexa RRID: AB_2535792 | Goat anti-Mouse | Gamma immunoglobins heavy and light chains | | Secondary, polyclonal | 1:200 |
| Goat anti-Rabbit IgG (H + L), Alexa Fluor Solomatic Rabbit IgG (H + L), Alexa Fluor Rabbit IgG (H + L), Alexa Rabbit IgG (H + L), | | | RRID: AB_2534069 | | |
| Donkey anti- Rabbit IgG (H + L), Alexa RID. AB_143137 Thermo Fisher Scientific, Secondary, polyclonal 1:200 Cat# A21206, RRID: AB_2535792 | Goat anti-Rabbit IgG (H + L), | Gamma immunoglobins heavy and light chains | | Secondary, polyclonal | 1:200 |
| Donkey anti- Gamma immunoglobins heavy and light chains Thermo Fisher Scientific, Secondary, polyclonal 1:200 Rabbit IgG (H + L), Alexa RRID: AB_2535792 | | | RRID: AB_143157 | | |
| INID. AD_2555772 | Donkey anti- Rabbit IgG | Gamma immunoglobins heavy and light chains | Cat# A21206, | Secondary, polyclonal | 1:200 |
| ***** | (H + L), Alexa Fluor 488 | | RRID: AB_2535792 | | |

Sigma Aldrich, St. Louis, USA; RRID: AB_476811) to assess the proliferation rate via BrdU incorporation. For visualization of primary antibodies, fluorescein-labeled anti-mouse immunoglobulin G (IgG), anti-rabbit IgG, or anti-goat IgG were used (dilution 1:200, Cat# A11001; RRID: AB_2534069, Cat#11011; RRID: AB_143157, Cat# A11057; RRID: AB_2534104, and Cat# A21206; RRID: AB_2535792, Thermo Fisher Scientific, Waltham, USA). All cells were counterstained with Hoechst 33342.

Pictures were taken using an inverted fluorescence phasecontrast microscope (Keyence-3000). All immunocytochemical experiments were performed in triplicate.

2.9 | Western blot analysis

For western blot analyses, astrocytes were sown and treated with CM in 6-well plates. Twenty-four hours after stimulation, cells were lysed and scraped using radioimmunoprecipitation assay-buffer containing proteinase and phosphatase inhibitors. Buffer containing the lysed cells was collected, and protein was separated by centrifuging. According to the manufacturer's protocol, 15 µg protein of each sample were applied to a 12% BisTris gel after determining protein concentrations with the Pierce bicinchoninic acid protein assay kit. After blotting on a nitrocellulose membrane, samples were stained for phospho-NFκB (Ser536, p65 antibody, rabbit monoclonal, dilution 1:1,000, Ca#MA5-15160, Thermo Fisher Scientific, Waltham, USA; RRID: AB 10983078) as well as for total NfkB (see above). Furthermore, phospho-p38 MAPK (Thr180/Tyr182; rabbit monoclonal antibody, Cat#4631, Cell Signaling Technology, Boston, USA; RRID: AB_331765) and total p38 MAPK (rabbit polyclonal antibody, dilution 1:500, Cat#9212, Cell Signaling Technology, Boston, USA; RRID: AB_330713) were detected. Anti-Histone H3 XP® (D1H2, rabbit monoclonal antibody, dilution 1:1,000, Cat#4499, Cell Signaling Technology, Boston, USA; RRID: AB_10544537) served as a loading control. Blots were visualized by peroxidase-linked secondary antibodies on a film.

2.10 | Oxygen-glucose deprivation

The culture medium of astrocytes was removed, and cells were gently rinsed with PBS to induce OGD. Cells were placed in a hypoxic chamber (Electrotek, Shipley, UK) with insufflation of gas containing 80% $\rm N_2$, 10% $\rm CO_2$, and 10% $\rm H_2$ at 37°C. Cells were covered with deoxygenated cell culture medium (DMEM) without glucose in the presence or absence of osteopontin. The oxygen concentration was below 0.1% throughout all experiments, as measured with an oxygen meter (GMH 3611-GL, Greisinger, Regenstauf, Germany). After 10 min, 1, 2, 3, 4, or 8 hr, cells were removed from the chamber for either an immediate live/dead assay or left to recover in fresh glucose- and oxygen-containing culture medium under normoxia (5% CO2) at 37°C. After 24 hr, those recovered cultures were used for live/dead assays, or RNA was extracted to perform RT-qPCR. Under control conditions, cells remained untreated.

2.11 | Migration assay

Cell migration was analyzed via scratch assay. After seeding on a 96-well plate and stimulation with CM in the presence or absence of osteopontin (5 and 10 μ g/ml), the well's floor with the adhering astrocytes was scratched with a sterile 200- μ l pipette tip. Brightfield images were recorded for up to 50 hr, and BZ analyzer was used for further analysis.

2.12 | Data processing and statistical analyses

Raw numerical data were processed with Microsoft Excel (Version 2016, Microsoft Corp., Seattle, WA, USA). All images were edited with Adobe Photoshop (Version CS2) by adjusting brightness, contrast, sharpness for each color channel, however, without exerting major modifications on images. ImageJ (version 1.52a) was used to switch the red and green color of the images shown in Figure 2c. Microsoft PowerPoint (Version 2016, Microsoft Corp.) and PDF creator (PDF24, pdfforge GmbH, Hamburg, Germany) were used to generate figures.

Statistical analyses were performed with IBM SPSS Statistics (Version 24, International Business Machines Corp. IBM, Armonk, USA), and graphics were created using GraphPad Prism (Version 6.01, GraphPad Software Inc., San Diego, CA, USA). Data are presented as scatter dot plots with a line indicating the mean value and standard deviation (SD). The migration assays are presented with superimposed symbols at mean value plus SD with a connecting line. The Supporting Information Figure S1f offers the affiliated scatter dot plots. To determine whether variables met the linear models' assumptions, Kolmogorov-Smirnov or Shapiro-Wilk tests for normal distribution and Levene's variance homogeneity test were performed. If all variables analyzed met the normality assumption, a t test or one-way analysis of variance (ANOVA) was conducted to compare multiple groups. An ANOVA was followed up by pairwise comparisons using the Tukey honest significant difference or Game's Howell test, used for variables with unequal variances. In case parameters turned out to be not normally distributed, the nonparametric Mann-Whitney U test (MWU) or, in case of comparing multiple groups, the Kruskal-Wallis test was calculated and followed up by Bonferroni correction. Statistical significance was assumed at less than the 5% level (p < 0.05).

3 | RESULTS

3.1 | Proinflammatory cytokines impact the function, phenotype, and expression pattern of primary astrocytes *in vitro*

The purity of the primary rat astrocyte culture was assessed by immunocytochemical staining for GFAP, expressed by >90% of all cells (Figure 1a). To obtain an active phenotype, astrocytes were treated

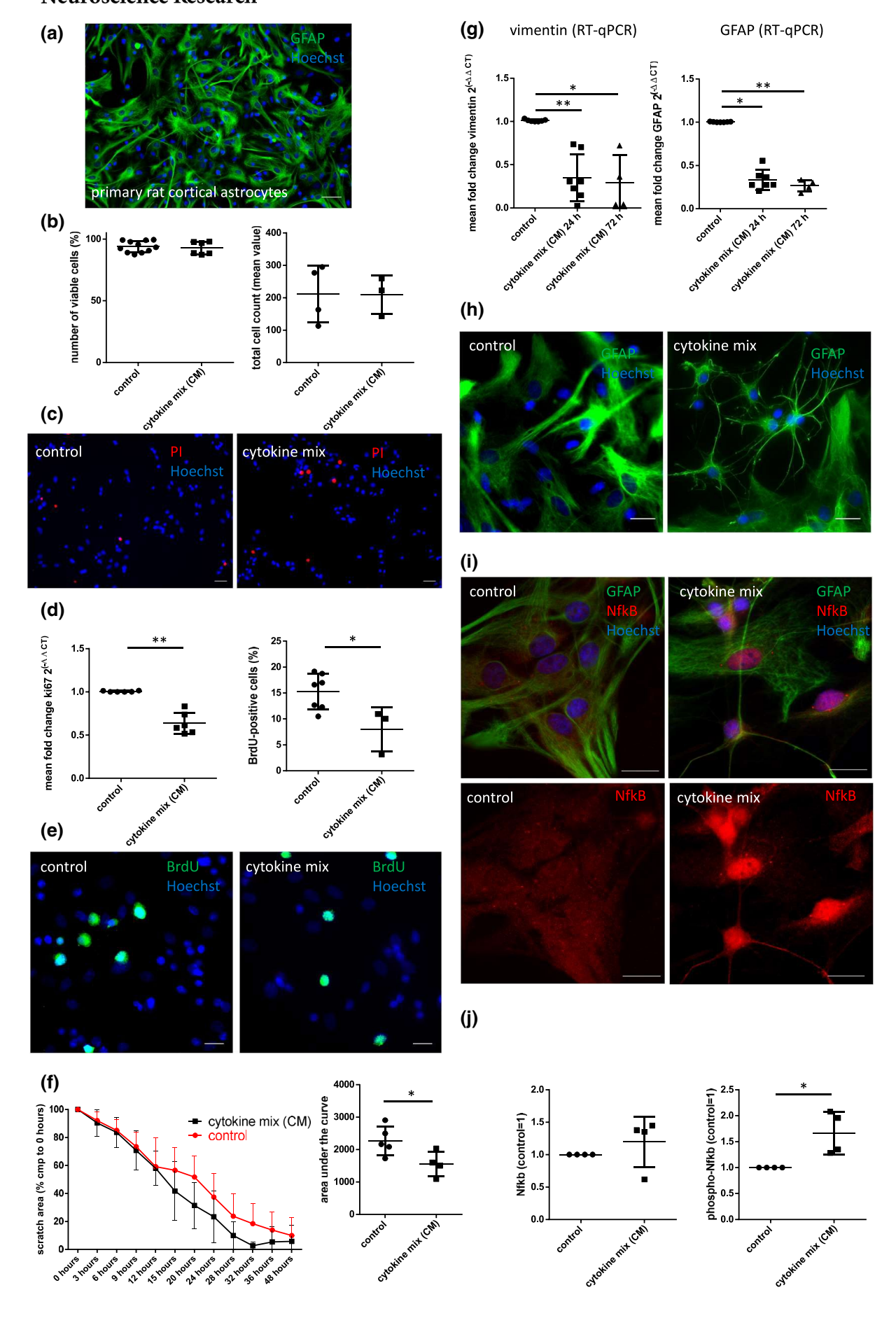


FIGURE 1 Function and morphology of primary resting and active astrocytes in vitro. *p < 0.05; **p < 0.01 compared different experimental groups as marked by a horizontal bar; each data point represents a biological experimental replicate with n = 3-11experimental replicates/group + standard deviations (SD). Each experimental replicate is the average value of three technical replicates with four pooled wells for RT-qPCR data; for live dead (B) and BrdU assay (D), each experimental replicate is the average value of two wells with ten field of views counted/well. For migration assay (F), each data point represents the mean value of three to seven biological experimental replicates/group/time point ± standard deviations (SD); for scatter plot, see Supporting Information Figure S1f. (a) Representative image depicting the homogenous culture of primary rat GFAP+ astrocytes (green) derived from rat cortices of newborns. Hoechst stained all cell nuclei blue, scale bar = 20 μm. (b) Ratio of viable astrocytes (in %; left panel) and total number of astrocytes per field of view (FOV; right panel) in the absence (control) or presence or of cytokine mix (CM, containing TNFα 10 ng/ml, IL1β 5 ng/ml, and IFNγ 10 ng/ml). Viable astrocytes were assessed by live/dead assay. (c) Representative images of the live/dead assay. All cells, regardless of their viability, were stained by Hoechst (blue), and dead cells were identified by propidium iodide (PI) incorporation (red); scale bars = 20 µm. (d) Proliferation rate after exposure to CM as assessed by ki67 expression (RT-qPCR; data are presented as mean fold change 2^(-ΔΔCT); left panel) and by BrdU incorporation (in %; right panel). (e) Representative images of the BrdU assay. Hoechst stained all cell nuclei blue, BrdU (green) identified proliferating cells; scale bars = $50 \mu m$. (f) Migration of astrocytes as assessed by scratch assay, in the absence (control) or presence of CM. Data were normalized to the scratch area at time point 0 hr in each experiment and condition (left panel). Supporting Information Figure S1f provides scatter plots for each condition. The scatter plot (right panel) depicts the area under the curve (AUC), illustrating enhanced astrocyte migration upon CM exposure. (g) Expression of the astrocytic markers vimentin and GFAP as measured by RT-qPCR in the absence (control) or presence of CM for 24 or 72 hr. Data are presented as $2^{(-\Delta\Delta CT)}$. (h) Representative immunocytochemical stainings of GFAP+ primary astrocytes (green) subjected to CM. Hoechst stained all cell nuclei blue; scale bar = 20 μm. (i) Upper row: representative immunocytochemical co-stainings of astrocytes against Nfkb (red) and GFAP (green) in the absence (control) and presence of CM. Lower row: exclusive depiction of the red channel illustrates the translocation of Nf κ B into the nucleus following CM exposure. Scale bars = 20 μ m. (j) Expression of NfxB and its phosphorylated active form assessed on the protein level by Western blot in control- and CM-exposed astrocytes. Data were normalized to loading control Histone H3 and untreated control = 1. For representative western blots see Supporting Information Figure S1a

with a mix of the proinflammatory cytokines TNF α , IL1 β , and IFN γ , known to be upregulated under neuroinflammatory conditions, for example, after cerebral ischemia (Walberer et al., 2010). We first aimed to characterize active astrocytes exposed to the proinflammatory cytokine mix (CM) for 24 hr, compared to unstimulated controls. The number of viable cells was 93.8% in the resting, and 92.7% in CM-treated astrocytes, demonstrating that the CM exerted no toxic effects on astrocytes (n = 6-11/group, t test: n.s.; Figure 1b,c). While absolute cell numbers were not affected by CM (n = 3-4/ group, MWU: n.s.; Figure 1b, right panel), the proliferation rate of astrocytes exposed to CM was significantly reduced, as measured by the expression of ki67 (0.36-fold in comparison to untreated control = 1; n = 6/group; MWU: p < 0.01; Figure 1d, left panel) and the BrdU-incorporation rate (8.1% with CM compared to 15.3% in the controls, n = 3-7/group, MWU: p < 0.05; Figure 1d, right panel and 1e).

A migration assay, establishing a central gap in a confluent astrocyte culture by a scratch with a pipette tip, and recording its repopulation by migrating cells at intervals for up to 48 hr, was used to assess proinflammatory cytokine effects on astrocyte migration. Under the influence of CM, astrocytes displayed a significant increase in migration, reflected by the area under the curve (AUC; 1,599 in the CM-treated group vs. 2,276 in the control group; n = 4-5/group, MWU: p < 0.05; Figure 1f). Notably, the effect of CM on astrocyte migration became detectable after 12 hr at the earliest. Also, we investigated the expression of two acknowledged markers of astrocyte activation, namely vimentin and GFAP, using RT-qPCR. Surprisingly, our data showed that-compared to control conditions-after both 24 and 72 hr of exposure to CM, primary rat astrocytes expressed less vimentin (0.35-fold at 24 hr, p < 0.01, and 0.29-fold at 72 hr, p < 0.05, control = 1, n = 4-7/group, Kruskal-Wallis test: H(3) = 11.03, p = 0.0005), and less GFAP (0.33-fold after

24 hr, p < 0.05, and 0.26-fold after 72 hr, p < 0.01; n = 4-7/group, Kruskal-Wallis test: H(3) = 10.15, p = 0.001; Figure 1g). Additionally, treatment with CM led to morphological changes in GFAP-positive astrocytes, forming condensed, radial, or bidirectional orientated cytoplasmatic processes (Figure 1h). Of note, the morphological changes affected only a part of astrocytes in the cell culture after treatment with CM (cf., to the lower part of the representative image of Figure 1h). Interestingly, regardless of the cell shape, CMstimulated astrocytes showed translocation of $Nf\kappa B$ into the nucleus (Figure 1i), suggesting an activation of the Nfkb signal transduction pathway, as only phosphorylated Nfkb can transfer the membrane of the nucleus. Corroborating this finding, we observed an upregulation of phosphorylated Nfkb after CM treatment (1.67-fold in comparison to untreated control = 1; n = 4/group; MWU: p < 0.05), while the expression of total Nfkb remained stable (n = 4/group, MWU: n.s.; Figure 1j). Of note, MAPK was not phosphorylated under the influence of CM (Supporting Information Figure S1a).

At the functional level, expression of inducible nitric oxide synthetase (iNOS) from astrocytes increased 26-fold upon CM exposure, compared to control ($n=7/{\rm group}$, MWU: p<0.001; Figure 2a, Supporting Information Figure S1b). At the same time, the proinflammatory cytokines IL6 and IL1ß were increased 3.4-fold (IL6; $n=8/{\rm group}$, MWU: p<0.01) and 6.9-fold (IL1ß; $n=7/{\rm group}$, MWU: p<0.001), compared to control (Figure 2a, Supporting Information Figure S1b). Expression of IL10 as an antiinflammatory cytokine was increased only by trend (~1.9-fold, $n=10/{\rm group}$, MWU: n.s.; Figure 2a, Supporting Information Figure S1b). As for the distinction between A1- and A2-activated astrocytes, exposure to CM led to a 1.6-fold upregulation of the designated A1-marker complement component 3 (CC3; $n=6/{\rm group}$, MWU: p<0.05), compared to control, as assessed by RT-qPCR (Figure 2a, Supporting Information Figure S1c). In contrast, mRNA expression of the A2-marker calcium-binding

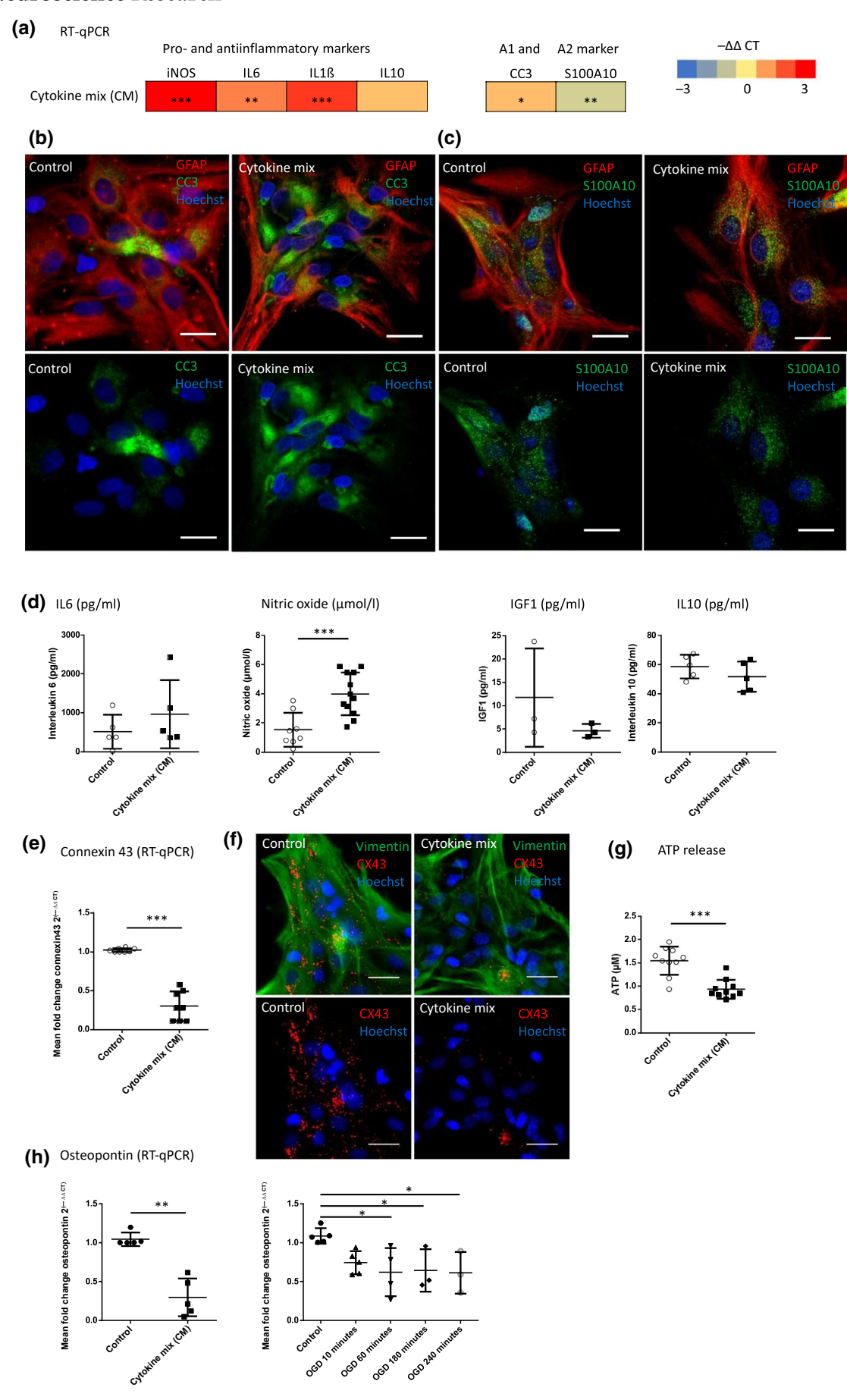


FIGURE 2 The secretory function and hemichannel activity of resting and active astrocytes. *p < 0.05; **p < 0.01; ***p < 0.001 compared to control; each data point represents a biological experimental replicate with n = 3-12 experimental replicates/group \pm standard deviations (SD). Each experimental replicate is the average value of three technical replicates with four pooled wells for RT-qPCR. For ELISA and Griess Assay each experimental replicate is the average value of three wells with two technical replicates/well. For ATP assay, each experimental replicate is the value of one well. (a) Heatmap of the pro- and antiinflammatory, as well as A1 and A2 marker expression, in primary astrocytes after exposure to cytokine mix (CM), assessed by RT-qPCR. Proinflammatory markers included inducible nitric oxide synthetase (iNOS) and the cytokines IL6 and IL1 β , while IL10 served as an antiinflammatory marker. Complement component 3 (CC3) characterized A1-activated, S100A10 the A2-activated astrocytes. Values are presented color coded as $-\Delta\Delta$ CT, compared to control astrocytes (in the absence of CM). For an extensive depiction of the data, cf., Supporting Information Figure S1b,c. (b) Upper row: representative immunocytochemical stainings of GFAP+ (red) and CC3+ (A1-activated) astrocytes (green) in the absence (control) or presence of CM. Lower row: exclusive depiction of the green channel to discern CC3. Hoechst stained all cell nuclei blue; scale bars = 20 µm. (c) Upper row: representative immunocytochemical stainings of GFAP+ (red) and S100A10+ (A2-activated) astrocytes (green) in the absence (control) or presence of CM. Lower row: exclusive depiction of the green channel to discern \$100A10. Hoechst stained all cell nuclei blue; scale bars = 20 µm. (d) Release of the proinflammatory mediators IL6 (first panel, ELISA) and nitric oxide (second panel, Griess Assay), and the antiinflammatory mediators insulin-like growth factor 1 (IGF1, third panel, ELISA) and IL10 (fourth panel, ELISA) in the absence (control) or presence of CM. (e) Expression of connexin 43 (CX43) RNA in the absence (control) or presence of CM. Data are presented as $2^{(-\Delta\Delta CT)}$. (f) Upper row: representative immunocytochemical stainings of astrocytes against vimentin (green) and CX43 (red); lower row: exclusive depiction of the red channel to discern CX43; Hoechst stained all cell nuclei blue; scale bars = 20 µm. (g) ATP release from astrocytes in the absence (control) or presence of CM. (h) Expression of osteopontin in astrocytes as measured on the RNA level by RT-qPCR. Data are presented as $2^{(-\Delta\Delta CT)}$; Left panel: osteopontin expression in the absence (control) or presence of CM. Right panel: osteopontin expression in astrocytes subjected to oxygen-glucose deprivation of varying duration with subsequent reoxygenation of 24 hr

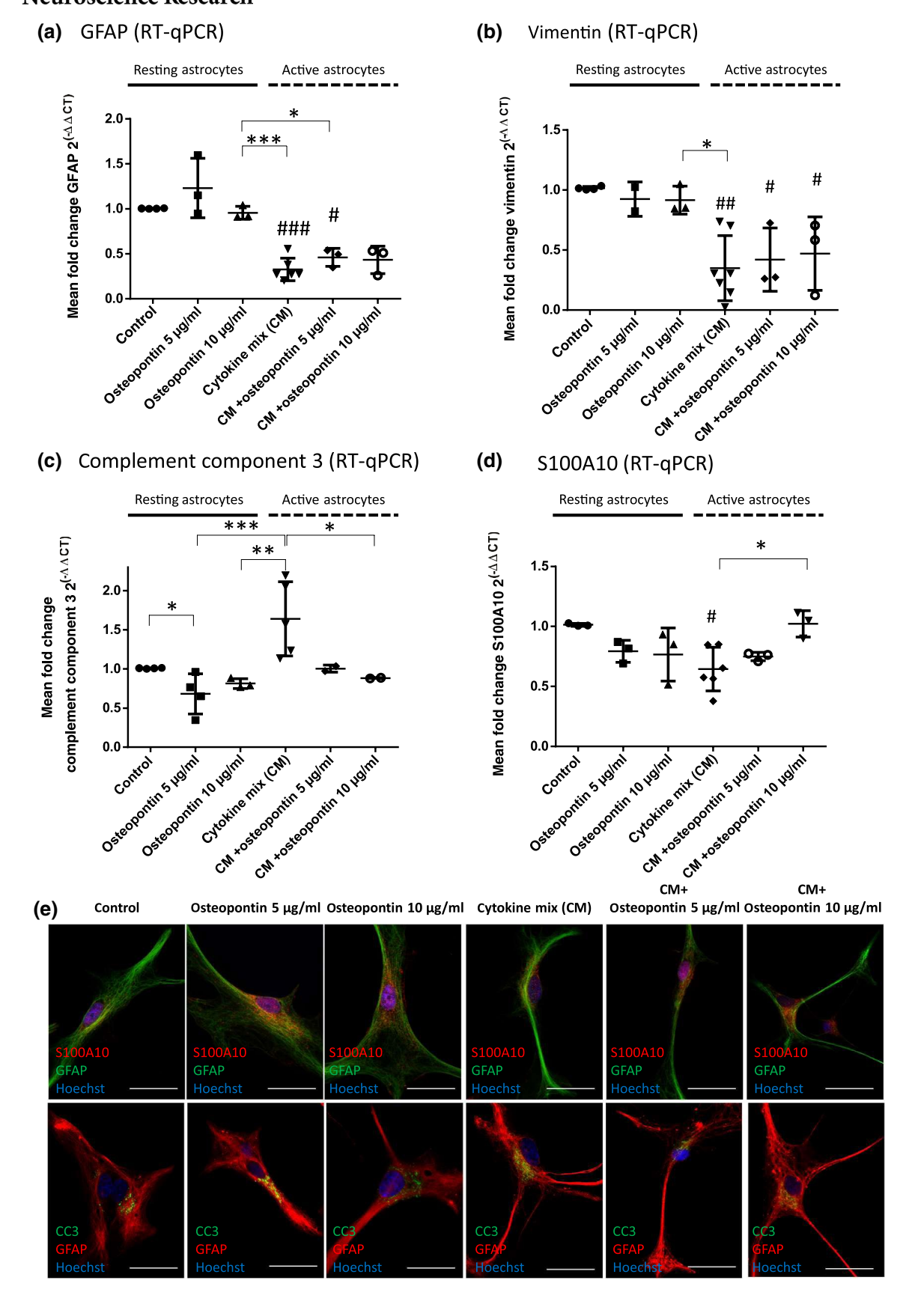
protein S100A10 was reduced 0.6-fold, compared to control (n = 5/ group, t test: p < 0.01; Figure 2a, Supporting Information Figure S1c). Immunocytochemical staining of astrocytes against CC3 and S100A10 protein revealed similar expression differences between control- and CM-exposed cells (Figure 2b,c). To further corroborate those findings on the mRNA level, secretion of the corresponding pro- and antiinflammatory cytokines, as well as nitric oxide (NO) release, were quantified from the supernatant of cultured astrocytes by ELISA and Griess Assay, respectively. Confirming the RT-qPCR results, CM induced the release of the proinflammatory cytokine IL6 (964 pg/ml vs. 516 pg/ml in the control group; n = 5/group, t test: n.s.)and of NO (3.98 μ M vs. 1.01 μ M in the control group; n = 8-12, t test: p < 0.001; Figure 2d). The release of the antiinflammatory proteins IL10 and IGF-1 from astrocytes was reduced only by trend, following exposure to CM (IL10: 51.7 pg/ml vs. 65.2 pg/ml in the control group, n = 4/group, t test: n.s.; IGF-1:4.6 pg/ml vs. 11.7 pg/ml in the control group, n = 3/group, MWU: n.s; Figure 2d). Astrocytes communicate with the extracellular space via releasing small molecules and ions forming hemichannels in their plasma membrane. Since hemichannels mainly consist of connexin 43 (CX43), we used CX43 expression as a surrogate for astrocyte hemichannel expression and assessed it on the mRNA level by RT-qPCR and the protein level by immunocytochemistry. Exposure to CM reduced CX43 expression in astrocytes by over 70%, compared to control (n = 8/group, t test: p < 0.001, Figure 2e,f). Likewise, ATP, reflecting astrocytic activity, is mainly released through hemichannels. ATP release was significantly decreased in astrocytes exposed to CM (0.93 μM vs. 1.56 μM in the control group, n = 10/group, t test: p < 0.001, Figure 2g). Finally, the endogenous expression of osteopontin mRNA was reduced in astrocytes exposed to CM (70% reduction compared to control, n = 5/group, MWU: p < 0.01; Figure 2h). Similarly, astrocytes subjected to oxygen-glucose deprivation (OGD) for 60-240 min with subsequent reoxygenation for 24 hr, an in vitro model of transient cerebral

ischemia, showed significantly reduced osteopontin mRNA expression, compared to control (p < 0.05; n = 3-5/group, ANOVA, post hoc Game's Howell test: (F(5,17) = 3.492; p = 0.0236); Figure 2h).

Overall, the characterization of primary astrocytes exposed to CM revealed significant structural and functional differences, compared to control cells, especially regarding morphology, marker expression, and immunocompetence. Therefore, we term the control cells "resting astrocytes" and the CM-exposed cells "active astrocytes" for the following experiments.

3.2 | Osteopontin regulates the activation phenotype but does not affect the immunocompetence of resting and active astrocytes

To assess the effects of osteopontin on resting and active astrocytes, we stimulated cells with osteopontin at 5 or 10 µg/ml, respectively. In resting astrocytes, osteopontin had no impact on the mRNA expression of GFAP and vimentin as markers of general activation (Figure 3a,b). In active astrocytes displaying reduced GFAP and vimentin mRNA expression (cf., Figure 1g), this low expression remained unchanged in the presence of osteopontin (Figure 1a,b; GFAP: n = 3-6/group, ANOVA, post hoc Game's Howell test: F(5,16) = 22.46; p = 0.0001; vimentin: n = 3-7/group, Kruskal-Wallis test: H(5) = 14.827; p = 0.011). However, after treatment with 5 µg/ ml osteopontin, expression of the A1 marker CC3 was reduced 0.68fold in resting astrocytes, compared to control (p < 0.05; Figure 3c,e). Furthermore, CM-induced upregulation of CC3 (cf., Figure 2a and Supporting Information Figure S1c) was counteracted by osteopontin (0.88-fold downregulation upon 10 µg/ml osteopontin, compared to control, p < 0.05; n = 2-5/group, Kruskal-Wallis test: H(5) = 16.917, p = 0.005, Figure 3c,e). In parallel, CM-induced downregulation of the A2 marker S100A10 was abolished by osteopontin



at 10 μ g/ml (0.64-fold downregulation upon 10 μ g/ml, compared to control, p < 0.05; n = 3-6/group, ANOVA, post hoc Game's Howell test: F(5, 15) = 4.29; p = 0.0001, Figure 3d,e).

We next investigated whether osteopontin affected the astrocytes' immunocompetence, that is, their function to produce pro- and antiinflammatory mediators. The panel of proinflammatory mediators

FIGURE 3 Osteopontin suppresses A1 while supporting A2 activation of astrocytes. In the following figures, astrocytes exposed to a cytokine mix (CM; TNF α 10 ng/ml, IL1 β 5 ng/ml and IFN γ 10 ng/ml) are termed "active," while unexposed astrocytes are termed "resting" (based on the data from Figures 1 and 2); *p < 0.05; **p < 0.01; ***p < 0.01; ***p < 0.001 compared to different experimental groups as marked by a horizontal bar; *p < 0.05; **p < 0.01; ***p < 0.001 compared to the control group; each data point represents a biological experimental replicate with p = 2-7 experimental replicates/group p = 1 standard deviations (SD). Each experimental replicate is the average value of three technical replicates with four pooled wells. RT-qPCR data are presented as p = 10. Characterization of resting and active astrocytes in the absence or presence of osteopontin, assessed by the expression of (a) GFAP (RT-qPCR) (b) vimentin (RT-qPCR) (c) CC3 (RT-qPCR) and (d) S100A10 (RT-qPCR). (e) Upper row: representative immunocytochemical stainings of astrocytes against S100A10 (red) and GFAP (green); lower row: representative immunocytochemical stainings of astrocytes against CC3 (green) and GFAP (red); Hoechst stained all cell nuclei blue; scale bars = 20 μ m

included iNOS, IL1ß, and IL6 (assessed on the mRNA level by RT-gPCR, for each: n = 3-7/group, Kruskal-Wallis test: n.s., Figure 4a-c), NO (assessed by Griess assay, n = 4-8/group, Kruskal-Wallis test: H(6) = 13.6; p = 0.0186, Figure 4d), and the cytokines IL1ß and TNF α (assessed on the protein level by ELISA, IL1 β : n = 3-6/group, ANOVA, post hoc Tukey honest test: F(5, 16) = 5.711; p = 0.0033; TNF α : n = 4-7/group, ANOVA, post hoc Game's Howell test: F(5, 27) = 104.2; p < 0.0001, Figure 4e,f). The panel of antiinflammatory mediators included IL10 (assessed on the mRNA as well as on the protein level (mRNA: n = 4-10/group, Kruskal-Wallis test: n.s.; protein: n = 2-6/group, Kruskal-Wallis test: n.s., Figure 4d,h) and IGF-1 (assessed on the protein level, n = 2-3/group, Kruskal-Wallis test: n.s., Figure 4i). Treatment of resting astrocytes with osteopontin at either concentration changed neither their production of proinflammatory (Figure 4a-f) nor of antiinflammatory mediators (Figure 4g-i). As detailed above, exposure of resting astrocytes to CM resulted in producing the proinflammatory mediators iNOS, IL6, IL1ß, and NO (cf., Figure 2a,d, Supporting Information Figure S1b). Corroborating this finding, active astrocytes showed upregulation of those proinflammatory mediators, compared to resting astrocytes (Figure 4a-c,e-g). Of note, the CM itself, used to induce active astrocytes, contained the cytokines TNF α and IL1 β . However, treatment with osteopontin at either concentration did not affect the production of proinflammatory (Figure 4a-c,e-g) or antiinflammatory mediators (Figure 4d,h,i) in active astrocytes, suggesting that their immunocompetence was not compromised by osteopontin. In line with these findings, immunocytochemical stainings of active astrocytes treated with osteopontin showed unaltered translocation of NfkB into the astrocytes' nucleus (Figure 4j, cf., Figure 1i).

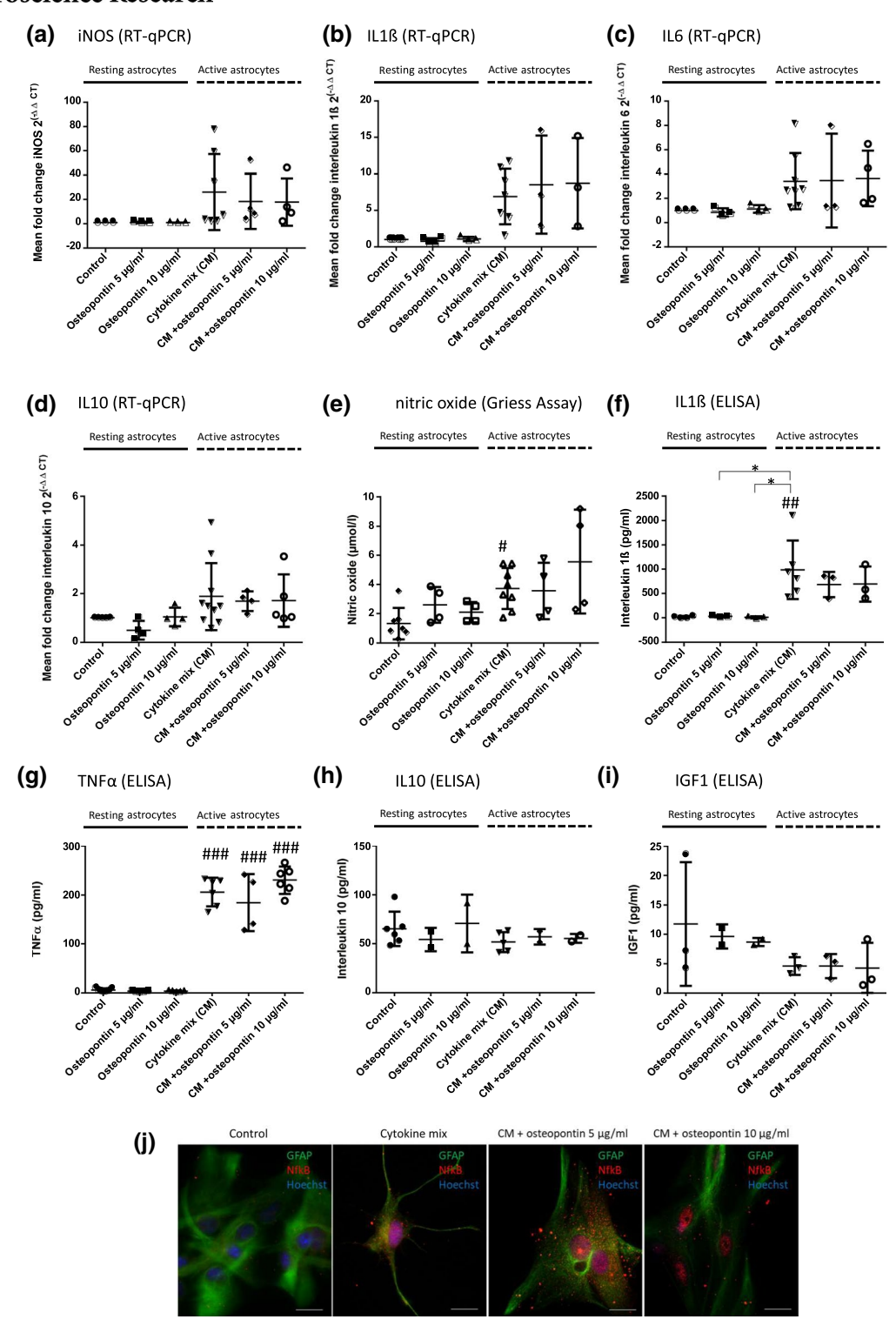
3.3 | Osteopontin enhances proliferation of active astrocytes and migration of resting astrocytes

Astrocytic proliferation was assessed by BrdU incorporation. In resting astrocytes, osteopontin only marginally enhanced proliferation (17.6% for 5 μ g/ml and 16.7% for 10 μ g/ml, compared to 15.3% in the absence of osteopontin, Figure 5a,c). As detailed above, active astrocytes exposed to CM displayed decreased proliferation (cf., Figure 1d,e). Interestingly, osteopontin abolished this effect (8.1% proliferation rate for active astrocytes, increased to 21% with 5 μ g/ml (p < 0.05), and to 20% with 10 μ g/ml osteopontin (n = 3–7/group, ANOVA post hoc Tukey honest test: F(5, 23) = 2.992; p = 0.0318; Figure 5a,c). Total cell count appropriately reflected the effects on proliferation

(Supporting Information Figure S1d; n=4-8/group, Kruskal-Wallis test: H(6) = 15.3; p=0.0092), and the live/dead assay confirmed that osteopontin had no negative effect on the survival of resting or active astrocytes (n=3-11/group, Kruskal-Wallis test: n.s., Figure 5b). As detailed above, active astrocytes—following exposure to CM—displayed enhanced migration, compared to resting astrocytes (cf., Figure 1f). Interestingly, osteopontin induced a similar effect in resting astrocytes and enhanced their migration into the central gap (AUC for 5 μ g/ml osteopontin: 1,295, compared to control: 2,276, p<0.01; n=5/group, ANOVA, post hoc Tukey honest test: F(2, 12) = 5.920, p=0.0163, Figure 6a,c). However, treatment of active astrocytes with osteopontin did not result in an additional increase in migration (n=4/group, ANOVA, post hoc Tukey honest test: n.s., Figure 6b,c).

3.4 | Osteopontin mitigates the ongoing death of astrocytes after a transient OGD

We used OGD as an in vitro model of cerebral ischemia to approximate osteopontin effects on astrocytes in ischemic stroke (cf., Figure 2h). Primary astrocytes were pre-conditioned with osteopontin for 24 hr, while untreated cells served as control. Then, all cells were subjected to OGD for 2, 4, or 8 hr in the presence of osteopontin (vs. control, as initiated before (Figure 7a). The ratio of dead astrocytes was measured by live/dead assay (1) immediately after OGD and (2) after astrocytes were allowed to recover from OGD for 24 hr under normoxia and normoglycemia (Figure 7a). Analyses immediately after OGD of various durations revealed a modest protective effect of osteopontin on astrocytes, displayed by a reduction in dead cells, especially after an OGD duration of 4 hr (5.14% without osteopontin vs. 1.98% and 2.86% with osteopontin, respectively; n = 6-7/group, ANOVA, post hoc Game's Howell test: F (2, 16) = 4.086, p = 0.0368, Figure 7b). Interestingly, when OGD was followed by a 24 hr recovery period under normal culture conditions, we observed astrocytes' ongoing death even during this recovery phase. This was most pronounced following the longest OGD duration of 8 hr, when astrocytes' death rate increased from 8.6% immediately after OGD to 33.9% 24 hr later (Figure 7b,c). Osteopontin, in particular, counteracted this delayed cell death, with the rate of dead cells decreasing from 33.9% to 18.8% by pre-conditioning with 5 µg/ ml osteopontin, and to 18.6% by pre-conditioning with 10 µg/ml osteopontin (both p < 0.05; n = 6-8/group, ANOVA, post hoc Game's Howell test: F(2, 19) = 4.394, p = 0.0270, Figure 7c,d).



4 | DISCUSSION

This study is the first to investigate *in vitro* the effects of osteopontin on survival, proliferation, migration, immunocompetence, and marker expression of resting astrocytes compared to astrocytes in an inflammatory milieu. Several years ago, Zamanian et al. postulated diverse types of activated astrocytes based on different gene expression profiles. Liddelow et al. recently categorized active

astrocytes into two different activation types, termed "A1" and "A2" (Liddelow & Barres B: SnapShot, 2015; Zamanian et al., 2012). A1 astrocytes upregulate many classical complement cascade genes destructive to synapses and exert cytotoxic effects on both neurons and oligodendrocytes (Liddelow et al., 2017). In contrast, A2 astrocytes upregulate neurotrophic factors and have been suggested to promote recovery and repair in the CNS (Bush et al., 1999; Sofroniew, 2015; Sofroniew & Vinters, 2010). These categories were

FIGURE 4 Osteopontin does not mitigate astrocytic immunocompetence. *p < 0.05 compared to different experimental groups as marked by a horizontal bar; *p < 0.05; *p < 0.01; *p < 0.001 compared to control group; each data point represents a biological experimental replicate with n = 2-8 experimental replicates/group \pm standard deviations (SD). Each experimental replicate is the average value of three technical replicates with four pooled wells for RT-qPCR. For ELISA and Griess Assay each experimental replicate is the average value of three wells with two technical replicates/well. (a–f) Regulation of specific proinflammatory mediators in resting and active astrocytes in the absence or presence of osteopontin on the RNA or protein level assessed by RT-qPCR (presented as $2^{(-\Delta \Delta CT)}$), Griess Assay and ELISA: (a) inducible nitric oxide- synthetase (iNOS) assessed by RT-qPCR (b) IL1ß assessed by RT-qPCR (c) IL6 assessed by RT-qPCR (d) Release of nitric oxide from resting and active astrocytes in the absence or presence of osteopontin as evaluated by Griess Assay (e) IL1ß measured by ELISA (f) TNF α measured by ELISA (g–i) Regulation of antiinflammatory mediators in resting and active astrocytes in the absence or presence of osteopontin on the RNA or protein level as assessed by RT-qPCR and ELISA: (g) IL10 assessed by RT-qPCR (h) IL10 measured by ELISA (i) IGF1 measured by ELISA (j) Representative immunocytochemical stainings of astrocytes against Nf α b (red) and GFAP (green) under resting conditions (first image) and after activation in the absence (second image) or presence of osteopontin at 5 α b (third image) or 10 α b (fourth image), respectively. Hoechst stained all cell nuclei blue; scale bars = 20 α b m

coined parallel to Th1 cells or M1 microglia, associated with excitotoxic inflammation, as opposed to regulatory and protective Th2 or M2 phenotypes, respectively. However, similar to microglia, which can simultaneously possess multiple active profiles and cannot simply be dichotomized into M1 and M2 microglia, A1 and A2 astrocytes most likely represent the two extremes of a continuous spectrum of activation profiles (Liddelow & Barres B: SnapShot, 2015; Vay et al., 2018).

In the present study, we chose TNF α , IL1 β , and IFN γ to activate resting astrocytes since those proinflammatory cytokines are highly expressed by CNS-resident microglia under neuroinflammatory conditions such as CNS infection, but also upon sterile neuroinflammation after a stroke or traumatic brain injury (Walberer et al., 2010). Compared to resting astrocytes, cells exposed to this proinflammatory cytokine mix revealed major differences in morphology (cf., Figure 1h), a reduced proliferation rate (cf., Figure 1d,e), enhanced migratory potential (cf., Figure 1f), strong expression of proinflammatory markers (cf., Figure 2a,d, Supporting Information Figure S1a,b), and reduced hemichannel activity (cf., Figure 2e-g). Moreover, astrocytes exposed to the cytokine mix increased the expression of complement component 3 (CC3) as a typical marker of A1 astrocytes while reducing the expression of S100A10 as an A2 marker (cf., Figure 2a,b, Supporting Information Figure S1c). Thus, we conclude that the used cytokine mix converted resting astrocytes to an active phenotype with A1 characteristics.

For decades, expression of GFAP has been used as a prototypic marker for the immunohistochemical identification of astrocytes, and an increase in GFAP expression has been associated with the formation of active gliosis after various brain injuries, for example, ischemic stroke, traumatic brain injury, or neurodegenerative diseases (Antanitus et al., 1975; Bignami et al., 1972; Burda et al., 2016; Potokar et al., 2020). At first sight counterintuitive to that, our active astrocytes decreased expression of GFAP and vimentin, that is, another marker associated with astrocyte activation, on the mRNA level (cf., Figure 1g,h). However, those findings are in line with other studies reporting at least an initial downregulation of GFAP expression on the mRNA level early after exposure to proinflammatory cytokines, followed by a late upregulation of GFAP on the protein level, as late as 24 hr after cytokine exposure

(Falsig et al., 2004, 2006). Moreover, in an attempt to induce A1 activation of astrocytes in vivo, Liddelow et al. injected lipopolysaccharides (LPS) into the cerebral ventricles of mice (Vay et al., 2018). This procedure induces a strong microglial activation and affects astrocytes indirectly via microglial signaling, due to their own shallow expression of the key LPS-receptor toll-like receptor 4 (Bowman et al., 2003; Sola et al., 2002). This procedure successfully induced a robust A1 activation phenotype in astrocytes, whichsimilar to our present study—displayed unchanged or even reduced expression of GFAP (Liddelow et al., 2017; Potokar et al., 2020). A priori, we have established matrix-free primary astrocyte cultures depleted of any other cell type or extracellular matrix (ECM) to assess mere astrocyte activation functionally. Therefore, the inflammatory stimuli might have evoked the surprising response of early and latent GFAP depression in our purified astrocyte cultures that differs from previous study results derived from more complex settings, usually in vivo experiments, in which various factors including microglia and ECM proteins influence the expression and drive GFAP mRNA to higher results.

One strength of our study is that it bridges the gap between previous studies on the concise transcriptional signature of resting and active astrocytes, on the one hand, and their critical functions, on the other hand, an approach with translational significance regarding the development of new therapeutic targets in neuroinflammation (Liddelow et al., 2020). Previous studies suggest that the function and reaction of the immune system and of brain cells—including astrocytes in health and disease—strongly depend on the organism's age (for review, see (Palmer & Ousman, 2018)). Therefore, one limitation of the present study is the exclusive use of primary astrocytes derived from neonatal rats.

Osteopontin is a pleiotropic protein highly expressed in the CNS during neuroinflammatory processes associated with infections (Brown et al., 2011; Jin et al., 2006), injury (Chan et al., 2014; Hashimoto et al., 2003; Li et al., 2017), ischemic stroke (Gliem et al., 2015; Rabenstein et al., 2019; Riew et al., 2019), and neoplasia (Szulzewsky et al., 2018). Osteopontin has even been suggested as a prognostic blood biomarker, for example, after hypoxic brain injury or trauma (Gao et al., 2020; Li et al., 2017). For the most part, osteopontin is derived from invading macrophages, monocytes, and resident microglia (Gliem

et al., 2015; Riew et al., 2019; Szulzewsky et al., 2018). *In vivo* data are sparse and imply an upregulation of osteopontin on the mRNA level in astrocytes in the early phase (d1-3) after an ischemic stroke (Rakers et al., 2019; Zamanian et al., 2012), with subsequent downregulation by day 7 (Choi et al., 2007; Zamanian et al., 2012). In contrast, in our primary astrocytes *in vitro*, both the proinflammatory cytokine mix and the exposure to OGD downregulated osteopontin on the mRNA level (cf., Figure 2h). This discrepancy between *in vitro* and *in vivo* findings may result from indirect effects involving, for example, intercellular cross-talk *in vivo*, and warrants further investigation.

Stimulation of active astrocytes with osteopontin attenuated the expression of the A1-marker CC3 and restored the expression of the A2-marker S100A10 (cf., Figure 3c-e). Based on this finding, we hypothesize that osteopontin may switch the phenotype of active A1 astrocytes towards an A2-activation type. This conjecture suggests parallels to microglia since M1-activated (neurotoxic) microglia lose their M1 competence upon osteopontin stimulation in vitro (Rabenstein et al., 2016), and exogenous application of osteopontin shifts microglia polarization toward the (neuroprotective) M2 phenotype after experimental ischemic stroke in vivo (Ladwig et al., 2017), modulating inflammatory responses toward regeneration (Ladwig et al., 2019; Schroeter et al., 2006). However, while osteopontin is known to modulate the expression of proand antiinflammatory cytokines from microglia in vitro and in vivo (Ladwig et al., 2017; Rabenstein et al., 2016; Schroeter et al., 2006; Tambuyzer et al., 2012), we here found no effect of osteopontin on the production of pro- or antiinflammatory mediators in astrocytes (cf., Figure 4). We interpret this as the astrocytes' ability to maintain their immunocompetence independent of subsequent signals, while microglia rather constitute versatile effector cells. Undoubtedly, this incongruity between microglial and astrocytic phenotypes and functionality stresses that a careful evaluation is needed to prevent oversimplification by transferring nomenclature between different types of glial cells.

In 2001, Chabas et al. first discussed osteopontin as a detrimentally acting proinflammatory agent. They and others showed that in mouse models of multiple sclerosis, the presence of osteopontin is necessary to induce recurrent relapses, worsen paralysis, and induce neurological deficits, including optic neuritis (Boggio et al., 2016; Chabas et al., 2001; Hur et al., 2007). These effects were mediated by enhancing myelin-reactive T cells' survival and proinflammatory function (Boggio et al., 2016; Chabas et al., 2001; Hur et al., 2007). On the other hand, other studies link osteopontin to regeneration and recovery of function (Cappellano et al., 2021). Lack of osteopontin in rodents has detrimental effects on lesion size, secondary neurodegeneration, and clinical outcome after cerebral ischemia or other CNS injury (Schroeter et al., 2006; Suzuki et al., 2010; Velthoven et al., 2011). The positive effects of osteopontin on brain repair after ischemic stroke are, at least in part, due to its effects on astrocytes to restore the blood-brain barrier by extending their astrocytic processes (Gliem et al., 2015). Another study revealed that the absence of osteopontin is associated with decreased proliferation of astrocytes after a brain lesion (Ikeshima-Kataoka et al., 2018). This finding is in line with our data, demonstrating osteopontin to completely restore the impaired proliferative capacity of active astrocytes (cf., Figure 5a,c). The proliferation of astrocytes plays a crucial role in regeneration as the basis of glial scar formation. protecting healthy tissue by distancing it from the necrotic area containing cytotoxic substances (Liu et al., 2014; Rolls et al., 2009). Thus, ablation of active astrocytes, for example, after spinal cord injury, is associated with a detrimental outcome (Faulkner et al., 2004). Of note, the glial scar is not only beneficial for recovery, since, at later stages of tissue remodeling, it may also block pivotal steps of repair and impede axon regeneration (Bush et al., 1999; Davies et al., 1999; Menet et al., 2003). However, it is currently assumed that not the astrocytic scar formation impairs recovery, but rather an improper timing of scar forming and scar resolution (Rolls et al., 2009; Shechter et al., 2011). Overall, the current study demonstrates robust effects of osteopontin on astrocytic proliferation. Our study thereby substantiates the high relevance of the interplay between osteopontin and active astrocytes in a neuroinflammatory milieu.

Given the known upregulation of osteopontin in ischemic brain tissue (Stoll et al., 1998) and to elaborate on the functional impact of osteopontin on astrocyte responses in CNS disease, we chose OGD as an in vitro model of ischemic stroke. OGD induced the immediate death of about 3.8%-8.6% of astrocytes, depending on its duration. Furthermore, the most substantial cell death of up to 34% occurred after astrocytes were allowed to recover for 24 hr under normoxic and normoglycemic conditions (cf., Figure 7b,c). We here report for the first time that pre-conditioning with osteopontin partly counteracts this OGD-induced delayed cell death in astrocytes (cf., Figure 7). Osteopontin is known to promote the survival of various cells, including bone marrow cells (Lin et al., 2000), dendritic cells (Kawamura et al., 2005), cancer cells (Lee et al., 2007), neural stem cells (Rabenstein et al., 2015), and microglia (Rabenstein et al., 2016). Besides, osteopontin was reported necessary for the survival of astrocytes in the retina (Ruzafa et al., 2018) or glioblastoma, conferring resistance to radiation (Friedmann-Morvinski et al., 2016). In vivo, osteopontin attenuates neuronal cell death via apoptotic pathways (Sun et al., 2019; Topkoru et al., 2013). Overall, our data on osteopontin promoting the survival of ischemia-inflicted astrocytes are relevant for a better understanding of stroke pathophysiology and the development of novel treatment approaches.

Osteopontin has multiple functional adhesive motifs that bind to various cell surface integrins and CD44 (Schroeter et al., 2006), induce different signaling pathways, and regulate a broad range of biological functions. The biological activity of osteopontin is modulated by proteolytic processing, which can reveal cryptic binding sites and remove or separate functional domains. One of the highly conserved motifs of osteopontin is the adhesive RGD domain that interacts with a variety of integrins including $\alpha v\beta 1$, $\alpha v\beta 3$, $\alpha v\beta 5$, $\alpha v\beta 6$, $\alpha 8\beta 1$, and $\alpha 5\beta 1$ integrins (Liaw et al., 1995; Yokosaki et al., 2005). Another part of the RDG motif is a cryptic SVVYGLR sequence that becomes exposed upon cleavage with thrombin and mediates interactions with $\alpha 9\beta 1$, $\alpha 4\beta 1$, and $\alpha 4\beta 7$ integrins (Green et al., 2001; Ito et al., 2009; Yokosaki

(a) BrdU-incorporation

(b) viable cells

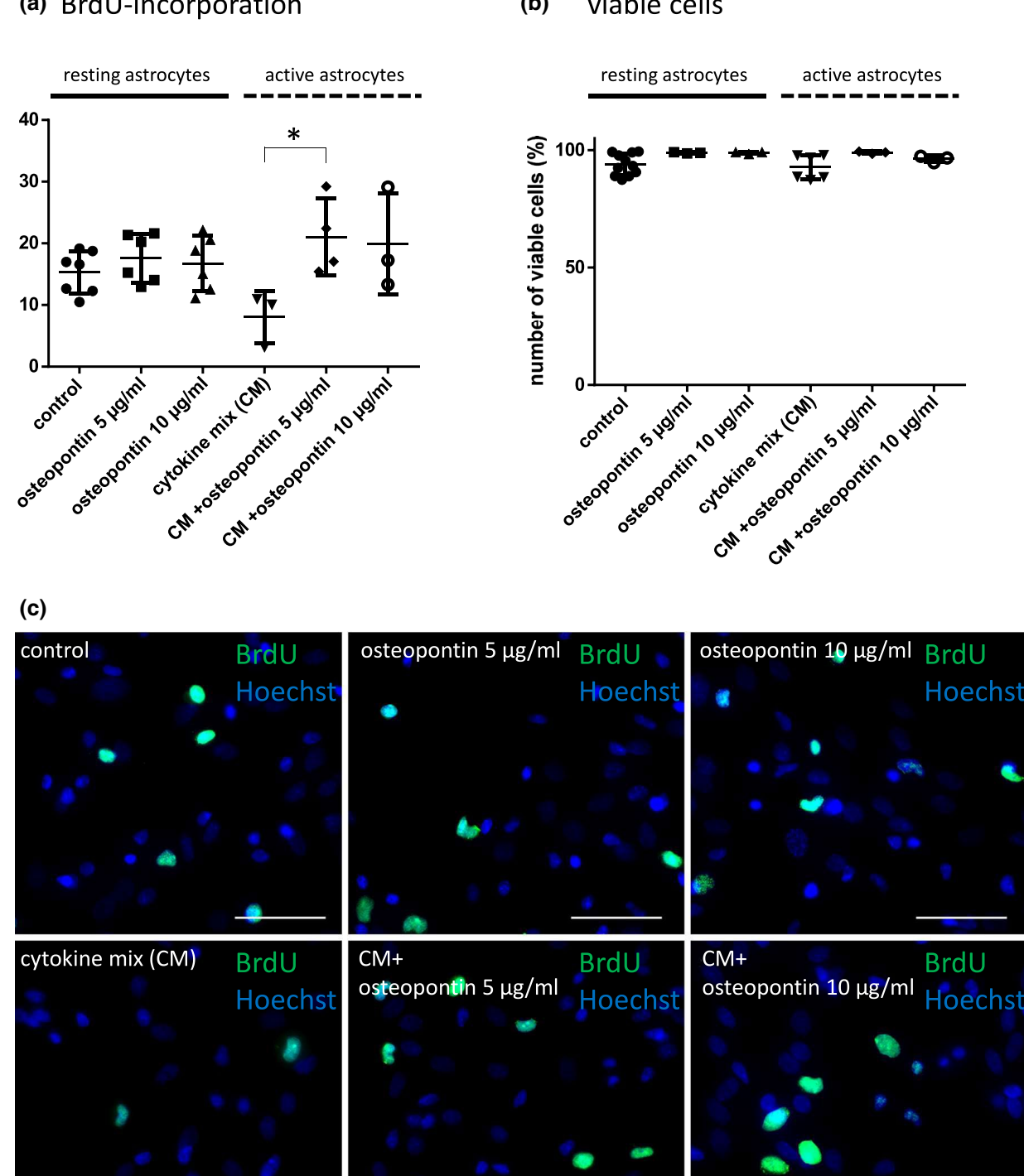


FIGURE 5 Osteopontin enhances the proliferation of active astrocytes. *p < 0.05 compared to different experimental group as marked by a horizontal bar; each data point represents a biological experimental replicate with n=3-11 experimental replicates/group \pm standard deviations (SD). Each experimental replicate is the average value of two wells with 10 field of views counted/well. (a) The proliferation rate of resting and active astrocytes was assessed by BrdU incorporation (in %) after treatment with osteopontin at 5 or 10 µg/ml. (b) The ratio of viable resting and active astrocytes after treatment with osteopontin at 5 or 10 µg/ml was assessed by live/dead assay. (c) Representative images of the proliferation assay identify BrdU+ proliferating astrocytes in green, all cell nuclei were counterstained with Hoechst; scale bars = $50 \mu m$

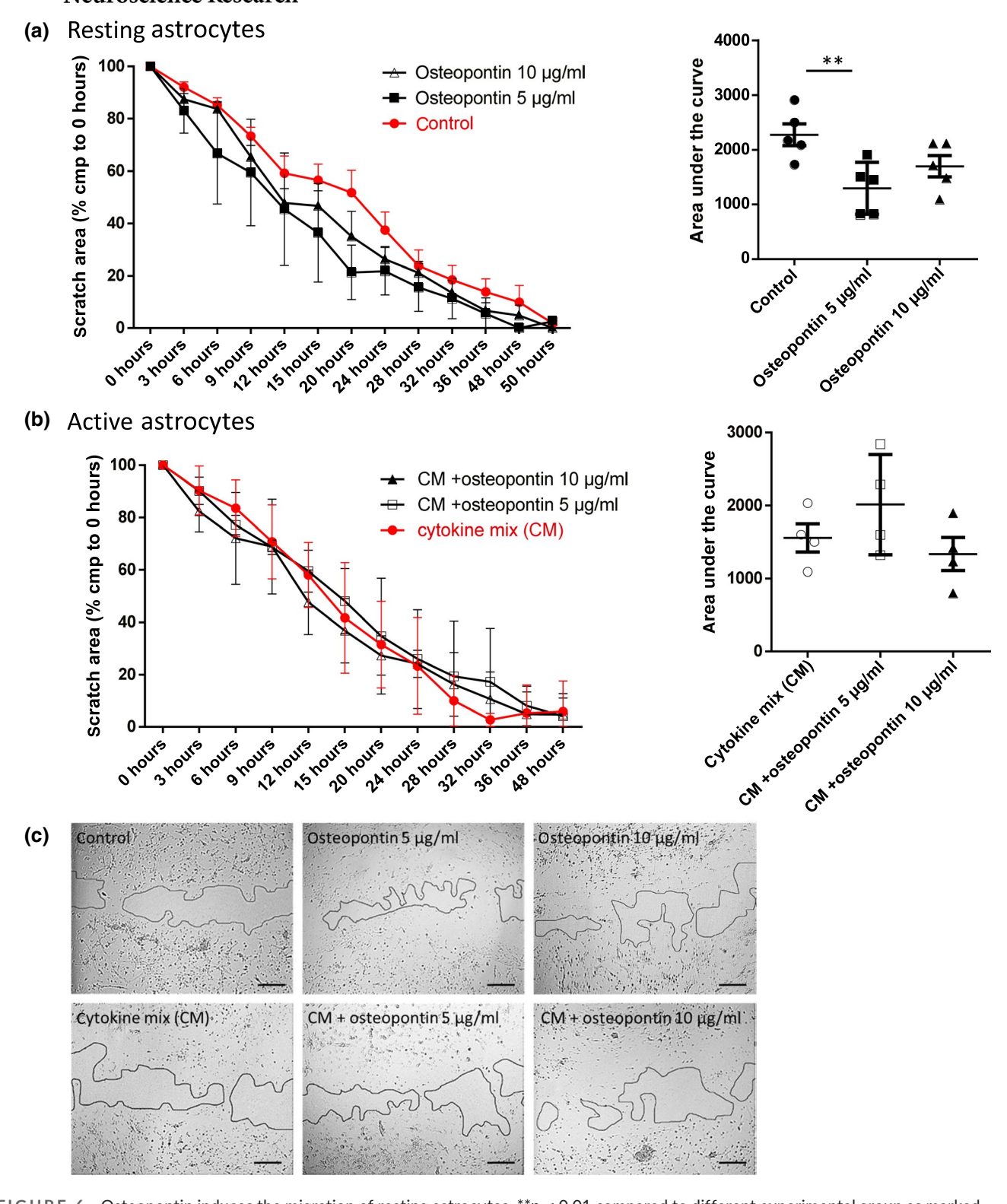


FIGURE 6 Osteopontin induces the migration of resting astrocytes. **p < 0.01 compared to different experimental group as marked by a horizontal bar; each data point represents the average value of n = 3-10 biological experimental replicates \pm standard deviations (SD). Supporting Information Figure S1f provides scatter plots for each condition, shown in A and B. (a) Migration of resting astrocytes as assessed by scratch assay, in the absence (control) or presence of osteopontin at 5 or 10 μ g/ml. Data were normalized to the scratch area at time point 0 hr in each experiment and condition (left panel). The boxplot (right panel) depicts the area under the curve (AUC) of each condition, illustrating enhanced astrocytic migration in the presence of 5 μ g/ml osteopontin. (b) Migration of active astrocytes as assessed by scratch assay, in the absence (cytokine mix) or presence of osteopontin at 5 or 10 μ g/ml. Data normalization and AUC calculation were performed as described above (6A). (c) Representative images of astrocyte cultures 24 hr after scratching, illustrating the repopulation of the central gap with astrocytes. Scale bars = 100 μ m

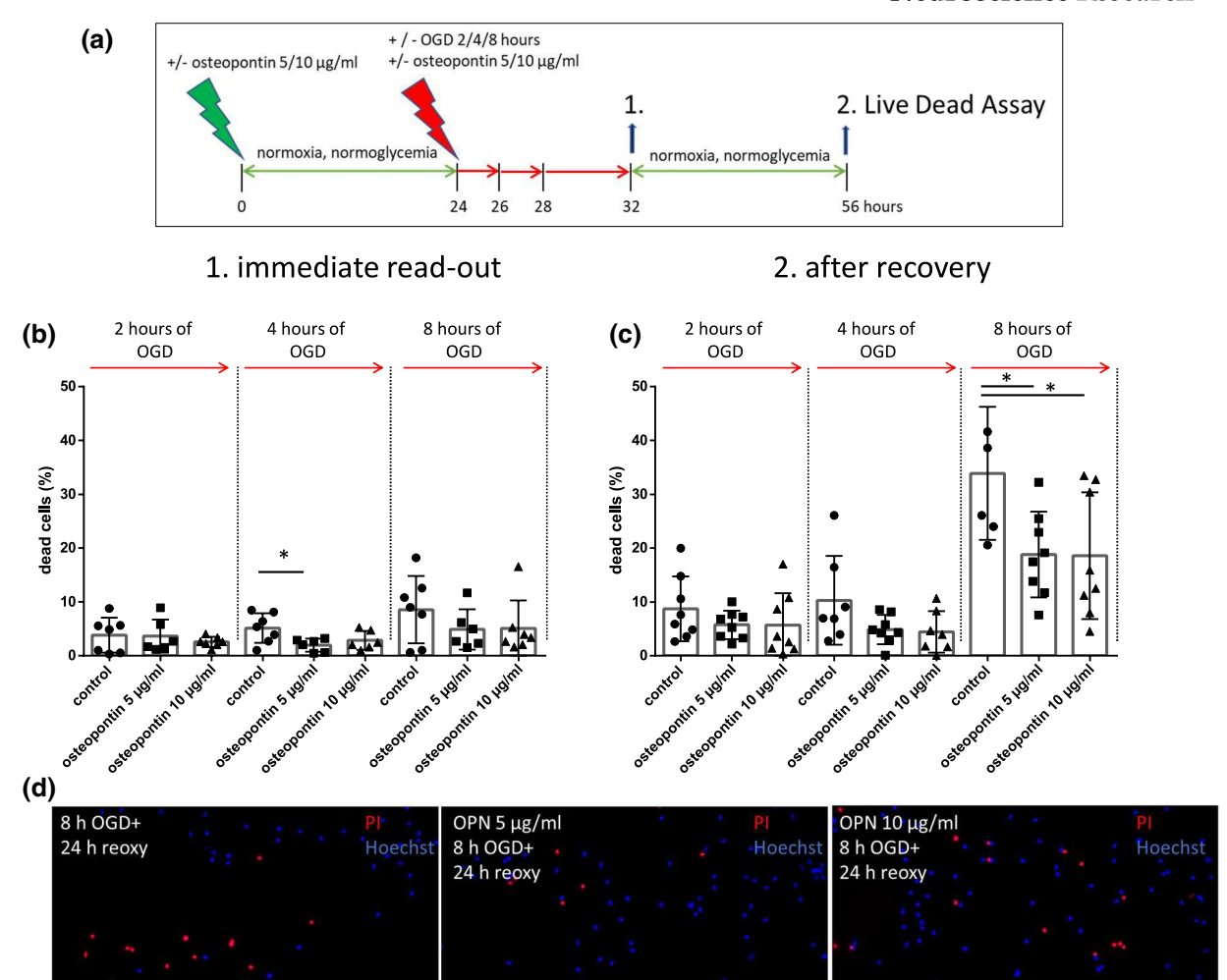


FIGURE 7 Osteopontin increases astrocyte survival upon deprivation of oxygen and glucose. *p < 0.05 compared to different experimental group as marked by a horizontal bar; each data point represents a biological experimental replicate with n = 3-12 experimental replicates/group \pm standard deviations (*SD*). Each experimental replicate is the average value of three wells with five field of views counted per well. (a) Schematic overview of the experimental setup. *Green thunderbolt*: astrocytes were pre-treated with osteopontin at 5 or 10 μ g/ml versus 0 μ g/ml (control) under normal cell culture conditions for 24 hr. *Red thunderbolt*: astrocytes were subjected to oxygen-glucose deprivation (OGD) for 2, 4, or 8 hr versus normal culture conditions (control) while being kept in the absence or presence of osteopontin as initiated before. *Immediate read-out* (1.): With some of the cells, a live/dead assay was performed immediately after OGD. *Delayed read-out* (2.): The remaining cells were reoxygenated under normoglycemic conditions for another 24 hr, followed by the live/dead assay. (b) Immediate read-out: The ratio of dead astrocytes following OGD for 2, 4, or 8 hr in the absence (control) or presence of osteopontin at 5 or 10 μ g/ml, assessed by live/dead assay immediately after OGD. (c) Read-out after recovery: After OGD in the absences or presence of osteopontin, astrocytes were reoxygenated under normoglycemic conditions for 24 hr, followed by live/dead assay. (d) Representative immunocytochemical live/dead assays of astrocytes subjected to OGD in the absence or presence of osteopontin. All cells, regardless of their viability, were stained by Hoechst (blue), and dead cells were identified by propidium iodide incorporation (red); scale bars = 100 μ m

et al., 1999). Furthermore, several different CD44 isoforms exist, and osteopontin can bind some CD44 splice variants, notably v6 and v7 (Katagiri et al., 1999; Smith et al., 1999). Furthermore, interactions between OPN and CD44 appears to be mediated via $\beta1$ integrins in an RGD independent manner (Katagiri et al., 1999). Of note, our experiments showed that there is not an apparent dose-effect correlation. Proliferation and migration even showed the maximal effect

of osteopontin in a lower dose (5 μ g/ml) in comparison to 10 μ g/ml (cf., Figures 5 and 6a). In line with this, in previous studies on serum-deprived microglia, we observed that the lower dose of osteopontin (6,25 μ g/ml) has an enhanced effect on cell survival than the higher dose of 12.5 μ g/ml (Briones-Orta et al., 2017). In contrast, our study reveals that the S100A10/CC3 expression was more affected when a higher dose of osteopontin was used (cf., Figure 3c,d), whereas the

effects of osteopontin on survival appeared to be independent of its dose (cf., Figure 7b). We speculate that the different effects of different doses of recombinant osteopontin on the biological functions of primary astrocytes might be due to inhomogeneous receptor-ligand binding affinities, sensitivities, and receptor saturation, dependent on the stimulated pathway. In this study, we did not evaluate the targeted cell signaling pathways. Therefore, additional studies are warranted to elucidate this issue further.

5 | CONCLUSION

Whereas its effects were subtle under resting conditions, osteopontin promoted migration, proliferation, and survival of primary astrocytes under stressful conditions *in vitro*. As contributed earlier, osteopontin is robustly upregulated and secreted in the extracellular space in several CNS conditions. It regulates microglial activation and promotes neuronal survival and blood-brain barrier function. Hence, we suggest osteopontin a vital determinant of the extracellular matrix milieu that plays a pivotal role in regulating degeneration and regeneration. Elucidating the interactions between osteopontin and astrocytes provides new insights into CNS pathophysiology and may facilitate the development of novel treatment approaches enhancing the endogenous regenerative capacity of the brain.

DECLARATION OF TRANSPARENCY

The authors, reviewers and editors affirm that in accordance to the policies set by the *Journal of Neuroscience Research*, this manuscript presents an accurate and transparent account of the study being reported and that all critical details describing the methods and results are present.

CONFLICT OF INTEREST

The authors declare that they have no competing interests.

AUTHOR CONTRIBUTIONS

Conceptualization and Project Administration, S.U.V.; Methodology, S.U.V., H.P., and E.G.; Investigation, S.U.V., D.N.O., H.P., F.L., E.G., M.R., N.N., and S.J.B.; Resources. S.U.V., M.A.R., M.S., and G.R.F.; Writing-Original Draft, S.U.V.; Writing-Review & Editing, M.A.R., M.S., and G.R.F; Supervision, M.A.R. and M.S.; Funding Acquisition, S.U.V., M.S., M.A.R., H.P., and G.R.F.

PEER REVIEW

The peer review history for this article is available at https://publo ns.com/publon/10.1002/jnr.24954.

DATA AVAILABILITY STATEMENT

The data that support the findings of this study are available from the corresponding author upon reasonable request.

REFERENCES

- Anderson, M. A., Burda, J. E., Ren, Y., Ao, Y., O'Shea, T. M., Kawaguchi, R., Coppola, G., Khakh, B. S., Deming, T. J., & Sofroniew, M. V. (2016). Astrocyte scar formation aids central nervous system axon regeneration. *Nature*, 532(7598), 195–200. https://doi.org/10.1038/nature17623
- Antanitus, D. S., Choi, B. H., & Lapham, L. W. (1975). Immunofluorescence staining of astrocytes in vitro using antiserum to glial fibrillary acidic protein. *Brain Research*, 89(2), 363–367. https://doi.org/10.1016/0006-8993(75)90729-5
- Bignami, A., Eng, L. F., Dahl, D., & Uyeda, C. T. (1972). Localization of the glial fibrillary acidic protein in astrocytes by immunofluorescence. *Brain Research*, 43(2), 429–435. https://doi.org/10.1016/0006-8993(72)90398-8
- Boggio, E., Dianzani, C., Gigliotti, C. L., Soluri, M. F., Clemente, N., Cappellano, G., Toth, E., Raineri, D., Ferrara, B., Comi, C., & Dianzani, U. (2016). Thrombin cleavage of osteopontin modulates its activities in human cells in vitro and mouse experimental autoimmune encephalomyelitis in vivo. *Journal of Immunology Research*, 2016, 9345495.
- Bowman, C. C., Rasley, A., Tranguch, S. L., & Marriott, I. (2003). Cultured astrocytes express toll-like receptors for bacterial products. *Glia*, 43(3), 281–291. https://doi.org/10.1002/glia.10256
- Briones-Orta, M. A., Avendano-Vazquez, S. E., Aparicio-Bautista, D. I., Coombes, J. D., Weber, G. F., & Syn, W. K. (2017). Osteopontin splice variants and polymorphisms in cancer progression and prognosis. *Biochimica Et Biophysica Acta (BBA) Reviews on Cancer*, 1868(1), 93–108.A. https://doi.org/10.1016/j.bbcan.2017.02.005
- Brown, A., Islam, T., Adams, R., Nerle, S., Kamara, M., Eger, C., Marder, K., Cohen, B., Schifitto, G., McArthur, J. C., Sacktor, N., & Pardo, C. A. (2011). Osteopontin enhances HIV replication and is increased in the brain and cerebrospinal fluid of HIV-infected individuals. *Journal of NeuroVirology*, 17(4), 382–392. https://doi.org/10.1007/s13365-011-0035-4
- Burda, J. E., Bernstein, A. M., & Sofroniew, M. V. (2016). Astrocyte roles in traumatic brain injury. *Experimental Neurology*, *275*(Pt 3), 305–315. https://doi.org/10.1016/j.expneurol.2015.03.020
- Bush, T. G., Puvanachandra, N., Horner, C. H., Polito, A., Ostenfeld, T., Svendsen, C. N., Mucke, L., Johnson, M. H., & Sofroniew, M. V. (1999). Leukocyte infiltration, neuronal degeneration, and neurite outgrowth after ablation of scar-forming, reactive astrocytes in adult transgenic mice. *Neuron*, 23(2), 297–308. https://doi.org/10.1016/50896-6273(00)80781-3
- Cappellano, G., Vecchio, D., Magistrelli, L., Clemente, N., Raineri, D., Barbero Mazzucca, C., Virgilio, E., Dianzani, U., Chiocchetti, A., & Comi, C. (2021). The Yin-Yang of osteopontin in nervous system diseases: Damage versus repair. Neural Regeneration Research, 16(6), 1131–1137. https://doi.org/10.4103/1673-5374.300328
- Chabas, D., Baranzini, S. E., Mitchell, D., Bernard, C. C., Rittling, S. R., Denhardt, D. T., Sobel, R. A., Lock, C., Karpuj, M., Pedotti, R., & Heller, R. (2001). The influence of the proinflammatory cytokine, osteopontin, on autoimmune demyelinating disease. *Science*, 294(5547), 1731–1735. https://doi.org/10.1126/science.1062960
- Chan, J. L., Reeves, T. M., & Phillips, L. L. (2014). Osteopontin expression in acute immune response mediates hippocampal synaptogenesis and adaptive outcome following cortical brain injury. Experimental Neurology, 261, 757–771. https://doi.org/10.1016/j.expneurol.2014.08.015
- Choi, J. S., Kim, H. Y., Cha, J. H., Choi, J. Y., & Lee, M. Y. (2007). Transient microglial and prolonged astroglial upregulation of osteopontin following transient forebrain ischemia in rats. *Brain Research*, 1151, 195–202. https://doi.org/10.1016/j.brainres.2007.03.016
- Chung, W. S., Clarke, L. E., Wang, G. X., Stafford, B. K., Sher, A., Chakraborty, C., Joung, J., Foo, L. C., Thompson, A., Chen, C., Smith,

- S. J., & Barres, B. A. (2013). Astrocytes mediate synapse elimination through MEGF10 and MERTK pathways. *Nature*, 504(7480), 394-400. https://doi.org/10.1038/nature12776
- Clarke, L. E., & Barres, B. A. (2013). Emerging roles of astrocytes in neural circuit development. *Nature Reviews Neuroscience*, 14(5), 311–321. https://doi.org/10.1038/nrn3484
- Davies, S. J., Goucher, D. R., Doller, C., & Silver, J. (1999). Robust regeneration of adult sensory axons in degenerating white matter of the adult rat spinal cord. *Journal of Neuroscience: The Official Journal of the Society for Neuroscience*, 19(14), 5810–5822. https://doi.org/10.1523/JNEUROSCI.19-14-05810.1999
- Falsig, J., Latta, M., & Leist, M. (2004). Defined inflammatory states in astrocyte cultures: Correlation with susceptibility towards CD95-driven apoptosis. *Journal of Neurochemistry*, 88(1), 181–193. https://doi.org/10.1111/j.1471-4159.2004.02144.x
- Falsig, J., Porzgen, P., Lund, S., Schrattenholz, A., & Leist, M. (2006). The inflammatory transcriptome of reactive murine astrocytes and implications for their innate immune function. *Journal of Neurochemistry*, 96(3), 893–907. https://doi.org/10.1111/j.1471-4159.2005.03622.x
- Faulkner, J. R., Herrmann, J. E., Woo, M. J., Tansey, K. E., Doan, N. B., & Sofroniew, M. V. (2004). Reactive astrocytes protect tissue and preserve function after spinal cord injury. *Journal of Neuroscience:* The Official Journal of the Society for Neuroscience, 24(9), 2143– 2155. https://doi.org/10.1523/JNEUROSCI.3547-03.2004
- Friedmann-Morvinski, D., Bhargava, V., Gupta, S., Verma, I. M., & Subramaniam, S. (2016). Identification of therapeutic targets for glioblastoma by network analysis. *Oncogene*, 35(5), 608–620. https://doi.org/10.1038/onc.2015.119
- Gao, N., Zhang-Brotzge, X., Wali, B., Sayeed, I., Chern, J. J., Blackwell, L. S., Kuan, C. Y., & Reisner, A. (2020). Plasma osteopontin may predict neuroinflammation and the severity of pediatric traumatic brain injury. *Journal of Cerebral Blood Flow and Metabolism*, 40(1), 35–43. https://doi.org/10.1177/0271678X19836412
- Giachelli, C. M., & Steitz, S. (2000). Osteopontin: A versatile regulator of inflammation and biomineralization. *Matrix Biology*, 19(7), 615–622. https://doi.org/10.1016/S0945-053X(00)00108-6
- Gliem, M., Krammes, K., Liaw, L., van Rooijen, N., Hartung, H. P., & Jander, S. (2015). Macrophage-derived osteopontin induces reactive astrocyte polarization and promotes re-establishment of the blood brain barrier after ischemic stroke. Glia, 63(12), 2198–2207. https://doi. org/10.1002/glia.22885
- Green, P. M., Ludbrook, S. B., Miller, D. D., Horgan, C. M., & Barry, S. T. (2001). Structural elements of the osteopontin SVVYGLR motif important for the interaction with alpha(4) integrins. FEBS Letters, 503(1), 75–79.
- Hashimoto, M., Koda, M., Ino, H., Murakami, M., Yamazaki, M., & Moriya, H. (2003). Upregulation of osteopontin expression in rat spinal cord microglia after traumatic injury. *Journal of Neurotrauma*, 20(3), 287–296. https://doi.org/10.1089/089771503321532879
- Huang, R. H., Quan, Y. J., Chen, J. H., Wang, T. F., Xu, M., Ye, M., Yuan, H., Zhang, C. J., Liu, X. J., & Min, Z. J. (2017). Osteopontin promotes cell migration and invasion, and inhibits apoptosis and autophagy in colorectal cancer by activating the p38 MAPK signaling pathway. *Cellular Physiology and Biochemistry*, 41(5), 1851–1864. https://doi.org/10.1159/000471933
- Hur, E. M., Youssef, S., Haws, M. E., Zhang, S. Y., Sobel, R. A., & Steinman, L. (2007). Osteopontin-induced relapse and progression of autoimmune brain disease through enhanced survival of activated T cells. *Nature Immunology*, 8(1), 74–83. https://doi.org/10.1038/ni1415
- Ikeshima-Kataoka, H., Matsui, Y., & Uede, T. (2018). Osteopontin is indispensable for activation of astrocytes in injured mouse brain and primary culture. Neurological Research, 40(12), 1071–1079. https:// doi.org/10.1080/01616412.2018.1517995
- Ito, K., Kon, S., Nakayama, Y., Kurotaki, D., Saito, Y., Kanayama, M., Kimura, C., Diao, H., Morimoto, J., Matsui, Y., & Uede, T. (2009). The

- differential amino acid requirement within osteopontin in alpha4 and alpha9 integrin-mediated cell binding and migration. *Matrix Biology*, 28(1), 11–19.
- Jin, J. K., Na, Y. J., Moon, C., Kim, H., Ahn, M., Kim, Y. S., & Shin, T. (2006). Increased expression of osteopontin in the brain with scrapie infection. *Brain Research*, 1072(1), 227–233. https://doi.org/10.1016/j.brainres.2005.12.013
- Katagiri, Y. U., Sleeman, J., Fujii, H., Herrlich, P., Hotta, H., Tanaka, K., Chikuma, S., Yagita, H., Okumura, K., Murakami, M., & Saiki, I. (1999). CD44 variants but not CD44s cooperate with beta1-containing integrins to permit cells to bind to osteopontin independently of arginine-glycine-aspartic acid, thereby stimulating cell motility and chemotaxis. Cancer Research, 59(1), 219–226.
- Kawamura, K., Iyonaga, K., Ichiyasu, H., Nagano, J., Suga, M., & Sasaki, Y. (2005). Differentiation, maturation, and survival of dendritic cells by osteopontin regulation. Clinical and Diagnostic Laboratory Immunology, 12(1), 206–212.
- Ladwig, A., Rogall, R., Hucklenbroich, J., Willuweit, A., Schoeneck, M., Langen, K. J., Fink, G. R., Rueger, M. A., & Schroeter, M. (2019). Osteopontin Attenuates Secondary Neurodegeneration in the Thalamus after Experimental Stroke. *Journal of Neuroimmune Pharmacology: the Official Journal of the Society on NeuroImmune Pharmacology*, 14(2), 295–311. https://doi.org/10.1007/s11481-018-9826-1
- Ladwig, A., Walter, H. L., Hucklenbroich, J., Willuweit, A., Langen, K. J., Fink, G. R., Rueger, M. A., & Schroeter, M. (2017). Osteopontin augments M2 microglia response and separates M1- and M2-polarized microglial activation in permanent focal cerebral ischemia. *Mediators of Inflammation*, 2017, 7189421. https://doi.org/10.1155/2017/7189421
- Lee, J. L., Wang, M. J., Sudhir, P. R., Chen, G. D., Chi, C. W., & Chen, J. Y. (2007). Osteopontin promotes integrin activation through outside-in and inside-out mechanisms: OPN-CD44V interaction enhances survival in gastrointestinal cancer cells. *Cancer Research*, 67(5), 2089-2097.
- Li, Y., Dammer, E. B., Zhang-Brotzge, X., Chen, S., Duong, D. M., Seyfried, N. T., Kuan, C. Y., & Sun, Y. Y. (2017). Osteopontin Is a blood biomarker for microglial activation and brain injury in experimental hypoxic-ischemic encephalopathy. *eNeuro*, 4(1), e0253-16.2016. https://doi.org/10.1523/ENEURO.0253-16.2016
- Liaw, L., Lindner, V., Schwartz, S. M., Chambers, A. F., & Giachelli, C. M. (1995). Osteopontin and beta 3 integrin are coordinately expressed in regenerating endothelium in vivo and stimulate Arg-Gly-Aspdependent endothelial migration in vitro. *Circulation Research*, 77(4), 665–672.
- Liddelow, S., & Barres, B. (2015). SnapShot: Astrocytes in health and disease. Cell, 162(5), 1170–1170 e1171. https://doi.org/10.1016/j. cell.2015.08.029
- Liddelow, S. A., Guttenplan, K. A., Clarke, L. E., Bennett, F. C., Bohlen, C. J., Schirmer, L., Bennett, M. L., Munch, A. E., Chung, W. S., Peterson, T. C., Wilton, D. K., Frouin, A., Napier, B. A., Panicker, N., Kumar, M., Buckwalter, M. S., Rowitch, D. H., Dawson, V. L., Dawson, T. M., ... Barres, B. A. (2017). Neurotoxic reactive astrocytes are induced by activated microglia. *Nature*, 541(7638), 481-487. https://doi.org/10.1038/nature21029
- Liddelow, S. A., Marsh, S. E., & Stevens, B. (2020). Microglia and astrocytes in disease: Dynamic duo or partners in crime? *Trends in Immunology*, 41(9), 820–835. https://doi.org/10.1016/j.it.2020.07.006
- Lin, Y. H., Huang, C. J., Chao, J. R., Chen, S. T., Lee, S. F., Yen, J. J., & Yang-Yen, H. F. (2000). Coupling of osteopontin and its cell surface receptor CD44 to the cell survival response elicited by interleukin-3 or granulocyte-macrophage colony-stimulating factor. *Molecular and Cellular Biology*, 20(8), 2734–2742. https://doi.org/10.1128/MCB.20.8.2734-2742.2000
- Liu, Z., Li, Y., Cui, Y., Roberts, C., Lu, M., Wilhelmsson, U., Pekny, M., & Chopp, M. (2014). Beneficial effects of gfap/vimentin reactive

- astrocytes for axonal remodeling and motor behavioral recovery in mice after stroke. *Glia*, 62(12), 2022–2033. https://doi.org/10.1002/glia.22723
- Matsumoto, T., Imagama, S., Hirano, K., Ohgomori, T., Natori, T., Kobayashi, K., Muramoto, A., Ishiguro, N., & Kadomatsu, K. (2012). CD44 expression in astrocytes and microglia is associated with ALS progression in a mouse model. *Neuroscience Letters*, 520(1), 115–120. https://doi.org/10.1016/j.neulet.2012.05.048
- Menet, V., Prieto, M., & Privat, A. (2003). Gimenez y Ribotta M: Axonal plasticity and functional recovery after spinal cord injury in mice deficient in both glial fibrillary acidic protein and vimentin genes. Proceedings of the National Academy of Sciences of the United States of America, 100(15), 8999–9004. https://doi.org/10.1073/pnas.1533187100
- Neal, M. L., Boyle, A. M., Budge, K. M., Safadi, F. F., & Richardson, J. R. (2018). The glycoprotein GPNMB attenuates astrocyte inflammatory responses through the CD44 receptor. *Journal of Neuroinflammation*, 15(1), 73.
- Oyama, M., Kariya, Y., Kariya, Y., Matsumoto, K., Kanno, M., Yamaguchi, Y., & Hashimoto, Y. (2018). Biological role of site-specific O-glycosylation in cell adhesion activity and phosphorylation of osteopontin. *The Biochemical Journal*, 475(9), 1583–1595. https://doi.org/10.1042/BCJ20170205
- Palmer, A. L., & Ousman, S. S. (2018). Astrocytes and aging. Frontiers in Aging Neuroscience, 10, 337. https://doi.org/10.3389/ fnagi.2018.00337
- Potokar, M., Morita, M., Wiche, G., & Jorgacevski, J. (2020). The diversity of intermediate filaments in astrocytes. *Cells*, *9*(7), 1604. https://doi.org/10.3390/cells9071604
- Rabenstein, M., Hucklenbroich, J., Willuweit, A., Ladwig, A., Fink, G. R., Schroeter, M., Langen, K. J., & Rueger, M. A. (2015). Osteopontin mediates survival, proliferation and migration of neural stem cells through the chemokine receptor CXCR4. Stem Cell Research & Therapy, 6, 99. https://doi.org/10.1186/s13287-015-0098-x
- Rabenstein, M., Unverricht-Yeboah, M., Keuters, M. H., Pikhovych, A., Hucklenbroich, J., Vay, S. U., Blaschke, S., Ladwig, A., Walter, H. L., Beiderbeck, M., Fink, G. R., Schroeter, M., Kriehuber, R., & Rueger, M. A. (2019). Transcranial current stimulation alters the expression of immune-mediating genes. Frontiers in Cellular Neuroscience, 13, 461. https://doi.org/10.3389/fncel.2019.00461
- Rabenstein, M., Vay, S. U., Flitsch, L. J., Fink, G. R., Schroeter, M., & Rueger, M. A. (2016). Osteopontin directly modulates cytokine expression of primary microglia and increases their survival. *Journal of Neuroimmunology*, 299, 130–138. https://doi.org/10.1016/j.jneuroim.2016.09.009
- Rakers, C., Schleif, M., Blank, N., Matuskova, H., Ulas, T., Handler, K., Torres, S. V., Schumacher, T., Tai, K., Schultze, J. L., Jackson, W. S., & Petzold, G. C. (2019). Stroke target identification guided by astrocyte transcriptome analysis. *Glia*, *67*(4), *619–633*. https://doi.org/10.1002/glia.23544
- Riew, T. R., Kim, S., Jin, X., Kim, H. L., Lee, J. H., & Lee, M. Y. (2019).

 Osteopontin and its spatiotemporal relationship with glial cells in the striatum of rats treated with mitochondrial toxin 3-nitropropionic acid: Possible involvement in phagocytosis.

 Journal of Neuroinflammation, 16(1), 99. https://doi.org/10.1186/s12974-019-1489-1
- Rogall, R., Rabenstein, M., Vay, S., Bach, A., Pikhovych, A., Baermann, J., Hoehn, M., Couillard-Despres, S., Fink, G. R., Schroeter, M., & Rueger, M. A. (2018). Bioluminescence imaging visualizes osteopontin-induced neurogenesis and neuroblast migration in the mouse brain after stroke. Stem Cell Research & Therapy, 9(1), 182. https://doi.org/10.1186/s13287-018-0927-9
- Rolls, A., Shechter, R., & Schwartz, M. (2009). The bright side of the glial scar in CNS repair. Nature Reviews Neuroscience, 10(3), 235–241. https://doi.org/10.1038/nrn2591

- Ruzafa, N., Pereiro, X., Aspichueta, P., Araiz, J., & Vecino, E. (2018). The Retina Of Osteopontin Deficient Mice In Aging. *Molecular Neurobiology*, 55(1), 213–221. https://doi.org/10.1007/s12035-017-0734-9
- Schroeter, M., Dennin, M. A., Walberer, M., Backes, H., Neumaier, B., Fink, G. R., & Graf, R. (2009). Neuroinflammation extends brain tissue at risk to vital peri-infarct tissue: A double tracer [11C]PK11195- and [18F]FDG-PET study. Journal of Cerebral Blood Flow and Metabolism, 29(6), 1216–1225.
- Schroeter, M., Zickler, P., Denhardt, D. T., Hartung, H. P., & Jander, S. (2006). Increased thalamic neurodegeneration following ischaemic cortical stroke in osteopontin-deficient mice. *Brain*, 129(Pt 6), 1426–1437. https://doi.org/10.1093/brain/awl094
- Shechter, R., Raposo, C., London, A., Sagi, I., & Schwartz, M. (2011). The glial scar-monocyte interplay: A pivotal resolution phase in spinal cord repair. *PLoS One*, 6(12), e27969. https://doi.org/10.1371/journ al.pone.0027969
- Smith, L. L., Greenfield, B. W., Aruffo, A., & Giachelli, C. M. (1999). CD44 is not an adhesive receptor for osteopontin. *Journal of Cellular Biochemistry*, 73(1), 20–30. https://doi.org/10.1002/(SICI)1097-4644(19990401)73:1<20:AID-JCB3>3.0.CO;2-3
- Sofroniew, M. V. (2015). Astrocyte barriers to neurotoxic inflammation. Nature Reviews Neuroscience, 16(5), 249–263. https://doi.org/10.1038/nrn3898
- Sofroniew, M. V., & Vinters, H. V. (2010). Astrocytes: Biology and pathology. *Acta Neuropathologica*, 119(1), 7–35. https://doi.org/10.1007/s00401-009-0619-8
- Sola, C., Casal, C., Tusell, J. M., & Serratosa, J. (2002). Astrocytes enhance lipopolysaccharide-induced nitric oxide production by microglial cells. *European Journal of Neuroscience*, 16(7), 1275–1283. https://doi.org/10.1046/j.1460-9568.2002.02199.x
- Song, H., Stevens, C. F., & Gage, F. H. (2002). Astroglia induce neurogenesis from adult neural stem cells. *Nature*, 417(6884), 39–44. https://doi.org/10.1038/417039a
- Stevens, B., Allen, N. J., Vazquez, L. E., Howell, G. R., Christopherson, K. S., Nouri, N., Micheva, K. D., Mehalow, A. K., Huberman, A. D., Stafford, B., & Sher, A. (2007). The classical complement cascade mediates CNS synapse elimination. *Cell*, 131(6), 1164–1178.
- Stoll, G., Jander, S., & Schroeter, M. (1998). Inflammation and glial responses in ischemic brain lesions. *Progress in Neurobiology*, *56*(2), 149–171. https://doi.org/10.1016/S0301-0082(98)00034-3
- Sun, C. M., Enkhjargal, B., Reis, C., Zhou, K. R., Xie, Z. Y., Wu, L. Y., Zhang, T. Y., Zhu, Q. Q., Tang, J. P., Jiang, X. D., & Zhang, J. H. (2019). Osteopontin attenuates early brain injury through regulating autophagy-apoptosis interaction after subarachnoid hemorrhage in rats. CNS Neuroscience & Therapeutics, 25(10), 1162–1172. https://doi.org/10.1111/cns.13199
- Suzuki, H., Hasegawa, Y., Kanamaru, K., & Zhang, J. H. (2010). Mechanisms of osteopontin-induced stabilization of blood-brain barrier disruption after subarachnoid hemorrhage in rats. *Stroke*, 41(8), 1783–1790. https://doi.org/10.1161/STROKEAHA.110.586537
- Szulzewsky, F., Schwendinger, N., Guneykaya, D., Cimino, P. J., Hambardzumyan, D., Synowitz, M., Holland, E. C., & Kettenmann, H. (2018). Loss of host-derived osteopontin creates a glioblastoma-promoting microenvironment. *Neuro-Oncology*, 20(3), 355–366. https://doi.org/10.1093/neuonc/nox165
- Tambuyzer, B. R., Casteleyn, C., Vergauwen, H., Van Cruchten, S., & Van Ginneken, C. (2012). Osteopontin alters the functional profile of porcine microglia in vitro. *Cell Biology International*, 36(12), 1233–1238.
- Topkoru, B. C., Altay, O., Duris, K., Krafft, P. R., Yan, J., & Zhang, J. H. (2013). Nasal administration of recombinant osteopontin attenuates early brain injury after subarachnoid hemorrhage. *Stroke*, 44(11), 3189–3194. https://doi.org/10.1161/STROKEAHA.113.001574
- van Velthoven, C. T., Heijnen, C. J., van Bel, F., & Kavelaars, A. (2011).

 Osteopontin enhances endogenous repair after neonatal

- hypoxic-ischemic brain injury. *Stroke*, 42(8), 2294–2301. https://doi.org/10.1161/STROKEAHA.110.608315
- Vay, S. U., Flitsch, L. J., Rabenstein, M., Rogall, R., Blaschke, S., Kleinhaus, J., Reinert, N., Bach, A., Fink, G. R., Schroeter, M., & Rueger, M. A. (2018). The plasticity of primary microglia and their multifaceted effects on endogenous neural stem cells in vitro and in vivo. *Journal of Neuroinflammation*, 15(1), 226. https://doi.org/10.1186/s1297 4-018-1261-y
- Walberer, M., Rueger, M. A., Simard, M. L., Emig, B., Jander, S., Fink, G. R., & Schroeter, M. (2010). Dynamics of neuroinflammation in the macrosphere model of arterio-arterial embolic focal ischemia: An approximation to human stroke patterns. Experimental & Translational Stroke Medicine. 2(1), 22.
- Wang, X., Louden, C., Yue, T. L., Ellison, J. A., Barone, F. C., Solleveld, H. A., & Feuerstein, G. Z. (1998). Delayed expression of osteopontin after focal stroke in the rat. *Journal of Neuroscience: The Official Journal of the Society for Neuroscience*, 18(6), 2075–2083. https://doi.org/10.1523/JNEUROSCI.18-06-02075.1998
- Yokosaki, Y., Matsuura, N., Sasaki, T., Murakami, I., Schneider, H., Higashiyama, S., Saitoh, Y., Yamakido, M., Taooka, Y., & Sheppard, D. (1999). The integrin alpha(9)beta(1) binds to a novel recognition sequence (SVVYGLR) in the thrombin-cleaved amino-terminal fragment of osteopontin. *Journal of Biological Chemistry*, 274(51), 36328-36334.
- Yokosaki, Y., Tanaka, K., Higashikawa, F., Yamashita, K., & Eboshida, A. (2005). Distinct structural requirements for binding of the integrins alphavbeta6, alphavbeta3, alphavbeta5, alpha5beta1 and alpha-9beta1 to osteopontin. *Matrix Biology*, 24(6), 418–427.
- Zamanian, J. L., Xu, L., Foo, L. C., Nouri, N., Zhou, L., Giffard, R. G., & Barres, B. A. (2012). Genomic analysis of reactive astrogliosis. Journal of Neuroscience: The Official Journal of the Society for Neuroscience, 32(18), 6391-6410.

SUPPORTING INFORMATION

Additional supporting information may be found online in the Supporting Information section.

FIGURE S1 (a) Data refer to the graphs in Figure 1j. Representative western blot images on the left side show the expression of Nf κ B, MAPK and their phosphorylated active forms in control- and CM-exposed astrocytes. Data were normalized to Histone H3 that served as loading control. On the right, uncropped blots are presented that refer to the graphs in Figure 1j. (a) and (c) Data refer to

the heat map results in figure 2A; *p < 0.05; **p < 0.01; ***p < 0.001 compared to controls; data are presented as $2^{(-\Delta\Delta CT)}$; each data point represents a biological experimental replicate with n = 5-10 experimental replicates/group ± standard deviations (SD). Each experimental replicate is the average value of three technical replicates with four pooled wells. (b) Expression of inducible nitric oxide synthetase (iNOS), the proinflammatory cytokines IL6 and IL1ß and the antiinflammatory cytokine IL10 in primary astrocytes after exposure to cytokine mix (CM) measured by RT-qPCR. (c) Expression of the A1-marker CC3 and the A2-marker S100A10 in primary astrocytes after exposure to cytokine mix (CM) as measured by RT-qPCR. (d) Representative immunocytochemical stainings of astrocytes against CX43 (red) and vimentin (green). Hoechst stained all cell nuclei blue; scale bars = $50 \mu m$. (e) Each data point represents a biological experimental replicate with n = 4-8 experimental replicates/group \pm standard deviations (SD). Each experimental replicate is the average value of two wells with 10 field of views counted/well. Total cell count of resting and activated astrocytes after exposure to osteopontin at 5 or 10 µg/ml. Data were normalized to untreated control. (f) Data refer to the graphs in figure 1 F, 6 A and B; each data point represents a biological experimental replicate with n = 3-10 experimental replicates/group \pm standard deviations (SD). Migration assay of resting and active astrocytes was assessed by scratch assay after treatment with osteopontin at 5 or 10 µg/ml. Data were normalized to the scratch area at time point 0 hours in each experiment and condition

Transparent Science Questionnaire for Authors Transparent Peer Review Report

How to cite this article: Vay, S. U., Olschewski, D. N., Petereit, H., Lange, F., Nazarzadeh, N., Gross, E., Rabenstein, M., Blaschke, S. J., Fink, G. R., Schroeter, M., & Rueger, M. A. (2021). Osteopontin regulates proliferation, migration, and survival of astrocytes depending on their activation phenotype. *Journal of Neuroscience Research*, 99, 2822–2843. https://doi.org/10.1002/jnr.24954